1965

Analogue measurement of charged particle trajectories in an inhomogeneous magnetic field.

Kelly, Patrick J.

Monterey, California: U.S. Naval Postgraduate School

ANALOGUE MEASUREMENT OF CHARGED PARTICLE TRAJECTORIES IN AN INHOMOGENEOUS MAGNETIC FIELD

PATRICK J. KELLY

ANALOGUE MEASUREMENT OF CHARGED PARTICLE TRAJECTORIES IN AN INHOMOGENEOUS MAGNETIC FIELD

* * *

Patrick J. Kelly

ANALOGUE MEASUREMENT OF CHARGED PARTICLE TRAJECTORIES IN AN INHOMOGENEOUS MAGNETIC FIELD

by

Patrick J. Kelly
//
Captain, United States Army

Submitted in partial fulfillment of
the requirements for the degree of

MASTER OF SCIENCE
IN
PHYSICS

United States Naval Postgraduate School
Monterey, California

1965

ANALOGUE MEASUREMENTS OF CHARGED PARTICLE TRAJECTORIES IN AN INHOMOGENEOUS MAGNETIC FIELD

by

Patrick J. Kelly

This work is accepted as fulfilling

the thesis requirements for the degree of

MASTER OF SCIENCE

IN

PHYSICS

from the

United States Naval Postgraduate School

ABSTRACT

The measurements described represent the first step in an experimental test of a classical impulse approximation for the capture process $H^+ + CH_4 \rightarrow H_2^+ + CH_3$. Since the predicted cross-sections in the applicable energy range are on the order of 10^{-18} cm^2 or less, the focussing properties of a thin lens beta ray spectrometer will be utilized to obtain maximum collection efficiency for the H_2^+ ions. The result of measuring the axial component of the magnetic field strength is given. A current-carrying wire was used to simulate the trajectories of the H_2^+ ions in the energy region 50-900 ev originating near the center of the magnet with a departure angle between 35 and 55^o with respect to the magnet axis. Measurements of the trajectories as well as the variation of departure angle with magnetic field strength at a fixed energy, $\left(\frac{\partial\theta}{\partial B}\right)_E$, were carried out.

TABLE OF CONTENTS

LIST OF ILLUSTRATIONS

SYMBOLS

θ - Scattering angle in laboratory frame, azimuthal angle used in orientation of magnetic field measurements

θ_c - Corrected or true particle departure angle

θ_m - Measured particle departure angle

$\textcircled{H}$ - Scattering angle in center of mass frame

φ - Angular coordinate of plane polar coordinate system

$d\alpha$ - Small angle subtending differential length ds

λ - Particle wavelength

ρ - Radius of curvature

μ - Reduced mass

B - Magnetic flux density

b - Scattering parameter

c - Speed of light in free space

D - Binding energy

E - Particle kinetic energy

ΔE - Uncertainty in energy

e - Electronic charge

f - An expression which is a function of the magnetic field strength and particle momentum, $\frac{eB}{2pc}$

g - Acceleration of gravity

$\hbar$ - $\frac{1}{2\pi}$ x Planck constant

I - Magnet current

i - Wire current

k - A constant, $2^{3/2} \pi m^{\frac{1}{2}}/e$

k - Pitch of spiral

L - Axial distance travelled by particle in one period corresponding to separation distance between angle and tension measuring instruments

M - Tension of wire in mass units, T/g

m - Particle mass

m_w - Mass of current carrying wire per unit length

$\vec{n}$ - Unit vector normal to current carrying wire

p - Particle momentum

Δp - Uncertainty in momentum

R - Radius of copper sleeve of angle measuring instrument

r - Radial distance from magnet axis, radial coordinate of plane polar coordinate system

r_a - Distance of closest approach

ds - Small segment of current carrying wire

T - Tension of wire in force units, period of revolution

$\vec{t}$ - Unit vector tangent to current carrying wire

dt - Differential time element

V - Potential energy

v - Particle velocity

$v_\perp$ - Component of particle velocity perpendicular to magnetic field

v_r - Relative velocity between two particles

Δx - Uncertainty in position

Z - Atomic number

z - Atomic number, distance along axis from center of magnet

1. Introduction

The data and results presented in this paper are part of an experimental project presently being conducted at the U. S. Naval Postgraduate School to verify a classical theory developed by Bates et. al. (1964a) for the capture of a light ion or atom from a target system by a fast projectile.

The particular reaction selected to be experimentally investigated is the capture of a hydrogen atom (H) by a fast proton (H^+) in its passage past a molecule of methane (CH_4). This can be conveniently written as

$$H^+ + HCH_3 \rightarrow H^+H + CH_3 \ . \qquad (1)$$

The energy range over which a classical description of this reaction is valid is examined. The de Broglie wavelength and Heisenberg uncertainty criteria, plus the additional condition that the energy of motion of H^+ relative to H must be less than the binding energy of the combined product H_2^+, limit the energy range to about 25-800 ev, and the scattering angle to the vicinity of 45 degrees.

The standard procedure of measuring the number of particles entering a detector placed at a definite scattering angle will not be feasible because of the expected low cross section (10^{-18} cm^2 or less). In order to obtain maximum counting efficiency, a thin lens beta ray spectrometer was selected which permits all particles coming out in a cone at a given scattering angle to enter the detector.

The axial component of the magnetic field was measured both along and off the axis with the results tabulated in Appendix 1. As was

expected, the field strength is linear with magnet current and is largest at the center. In order to provide insight into the positioning of the interaction chamber, the detector, the various baffles, it was necessary to have some information concerning the trajectory of the H_2^+ particle. This was done by simulating the particle path by a flexible current-carrying wire in the magnetic field. It is shown that the wire takes up a position coincident with the orbit of the charged particle provided that the current and tension of the wire are adjusted to correspond to the energy of the particle in question through the expression

$$E^{\frac{1}{2}} = 48 \frac{M}{i} \qquad (2)$$

where E is the energy of the H_2^+ particle (also that of the incoming H^+), M is the tension of the wire in mass units, and i is the wire current. Wire trajectories corresponding to particles having energies from 50-900 ev and leaving the magnet axis with angles from 35-55 degrees are examined and tabulated in Appendix 4. The variation of the particle departure angle with respect to the magnetic field strength at constant energy $\left(\frac{d\theta}{dE}\right)_E$ is also calculated from the experimental data. All of the trajectory work was done with the wire leaving the axis near the center of the magnet and focussing at a fixed distance approximately 40 cm down axis. It was experimentally determined that optimum trajectories occurred between these two points.

At the present time a theoretical analysis of the particle trajectories in the same energy and angular ranges is in progress. It is hoped that these numerical computations will substantiate the experimental data given in this paper.

2. Theory

(a) Impulse Approximation

Since a quantum mechanical treatment is not possible for any but the very simplest atomic interactions, the use of approximate solutions, particularly semiclassical, become important.

The impulse approximation states that for high energies where polarization forces and chemical binding of the colliding particles may be ignored, the components of a complex system interact independently of each other. Furthermore, under certain conditions, classical theory may be used to examine the interaction and predict cross sections.

We shall be concerned with the following ion-molecule rearrangement collision which can be handled experimentally

$$\underline{H}^+ + CH_4 \rightarrow \underline{H_2}^+ + CH_3 \qquad (3)$$

and more conveniently written as

$$\underline{H}^+ + HCH_3 \rightarrow \underline{H^+H} + CH_3$$

where the underlined terms represent particles having considerable kinetic energy in the laboratory frame.

Using Fig. 1 as portraying the capture mechanism, the reaction is briefly described in the following manner. H (a hydrogen atom) initially bound to CH_4 (a methane molecule) suffers a binary collision with H^+ (the proton) and then suffers another binary collision with C (the carbon atom). Classical kinematics predicts that H^+ and the doubly scattered H will have a small relative velocity such that there is a large probability that the two particles will be bound and emerge as an H_2^+ particle.

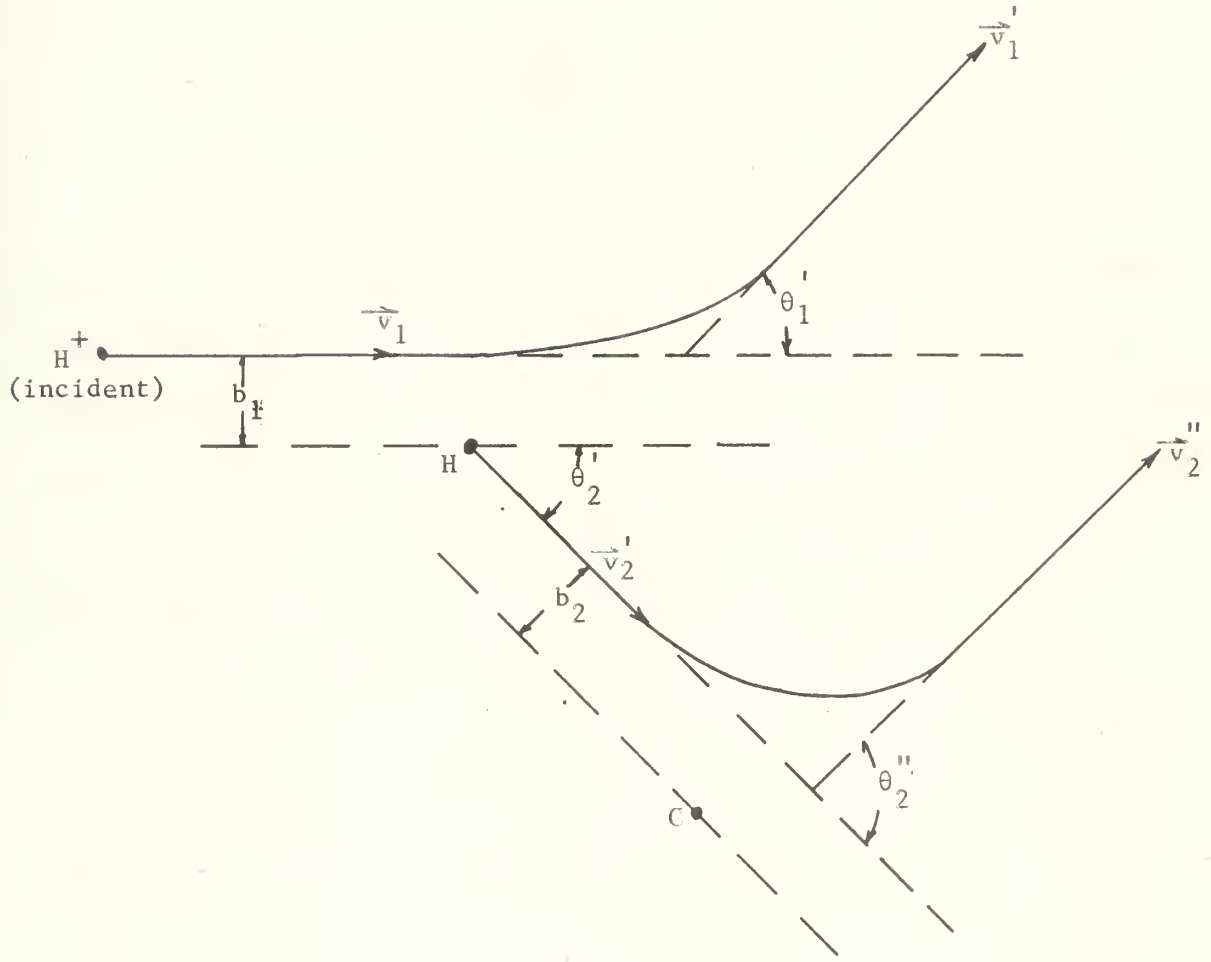

Fig. 1

Hydrogen Atom Capture Mechanism in Laboratory Frame

If the assumption is made that the nucleus of C is infinitely heavy, then in the laboratory frame

$$\theta_1' \simeq 45^\circ \ , \ \theta_2' \simeq 45^\circ \ , \ \theta_2'' \simeq 90^\circ$$

and (4)

$$v_1' \simeq v_2' \simeq v_2'' \simeq \frac{v_1}{\sqrt{2}} \ .$$

It is important for both theoretical and experimental reasons to determine over what energy range this classical concept is valid. The requirements that must be satisfied are the usual de Broglie wavelength limitations and Heisenberg uncertainty relations for both binary collisions plus the additional requirement that the uncertainty in the final value of the energy of motion of H^+ relative to H must be less than D, the binding energy of the final reaction product H_2^+.

One of the conditions for the use of a classical description specifies that the wavelength λ of any particle involved must be much less than the smallest distance involved in the collision which, in this case, is the distance of closest approach r_a, or

$$\lambda \ll r_a \tag{5}$$

For elastic scattering in a central force field, an analysis such as that given by McDaniel (1964b) shows that r_a may be derived from the scattering parameter b in the following manner. In the center of mass system b is given by the expression

$$b = \frac{Z\, z\, e^2}{\mu\ v_r^2} \cot \frac{\Theta}{2} \tag{6}$$

where Z and z are the atomic numbers of the colliding particles, μ is the reduced mass of the system, v_r is the relative velocity between the particles, and Θ is the scattering angle.

For the H^+ - H collision,

$$\mu = \frac{m_H}{2} \quad \text{and} \quad \Theta_2' \simeq \pi/2 \tag{7}$$

and for the H - C collision,

$$\mu \simeq m_H \quad \text{and} \quad \Theta_2'' \simeq \pi/2 \ . \tag{8}$$

Making these substitutions in (6) we obtain

$$b_{H^+-H} = \frac{e^2}{E} \quad \text{and} \quad b_{H-C} = \frac{6\,e^2}{E} \tag{9}$$

where E is the kinetic energy of the incident H^+ in the laboratory frame. Because of different velocities, E is also the kinetic energy of the H_2^+ particle after the interaction.

The distance of closest approach r_a can be found as the largest real root of the equation

$$1 - \frac{V(r_a)}{\left(\frac{\mu\, v_r^2}{2}\right)} - \frac{b^2}{r_a^2} = 0 \tag{10}$$

where $V(r_a)$ is the Coulomb potential evaluated at r_a. Substituting (9) into (10) we obtain

$$r_{a_{H^+-H}} = \frac{2.42\ e^2}{E} \quad \text{and} \quad r_{a_{H-C}} = \frac{14.5\ e^2}{E} \ . \tag{11}$$

It is therefore seen that $r_{a_{H^+-H}}$ is the limiting dimension to be used for the de Broglie wavelength criterion. To satisfy this requirement we take

$$\lambda = \frac{\hbar}{m_H v_1} = 1/10\ r_{a_{H^+-H}} \tag{12}$$

whereby we obtain $v_1 = 1.69 \times 10^6$ cm/sec corresponding to an incident H^+ kinetic energy of 150 ev. As $\lambda \propto \frac{1}{v}$ and $r_a \propto \frac{1}{v^2}$, it is seen that r_a will decrease faster than λ, and thus this value represents an upper limit on the energy.

The second requirement for the application of classical theory applies the restrictions imposed by the Uncertainty Principle. The uncertainty in energy ΔE introduced by specifying the transverse position of the particle must be small compared to the binding energy of the final product. If the maximum uncertainty in the transverse direction is Δx, and in momentum is Δp, then this requirement can be written as

$$\Delta p \Delta x = \frac{\hbar^2}{2} \ . \tag{13}$$

However as

$$\Delta E = \frac{\Delta p^2}{2m_H} \tag{14}$$

we obtain

$$\Delta E = \frac{\hbar^2}{8m_H (\Delta x)^2} \tag{15}$$

and since

$$\Delta x < r_a \tag{16}$$

we have

$$\Delta E > \frac{\hbar^2}{8m_H r_a^2} \quad . \tag{17}$$

In addition ΔE should be small compared to D, and we can finally write this requirement as

$$D \gg \frac{\hbar^2}{8m_H r_{a_{H^+-H}}^2} \tag{18}$$

using $r_{a_{H^+-H}}$ as the smallest distance of closest approach involved.

Again using a factor of 10, we require that

$$D = \frac{10\hbar^2}{8m_H r_{a_{H^+-H}}^2} \quad . \tag{19}$$

Substituting (11) into (19) and solving for the incident H^+ kinetic energy, we find

$$E = \frac{2.42\ e^2 \sqrt{8m_H D}}{\sqrt{10}\ \hbar} \tag{20}$$

where D is 2.6 ev for an H_2^+ particle. Putting in the proper values, one calculates $E = 820$ ev as satisfying this condition. As in the de Broglie wavelength criterion, this value also places an upper limit on the incident H^+ energy.

There exists, however, one further peculiarity which should be mentioned. Bohm (1951) shows that for a strictly Coulomb potential, the classical (Rutherford) cross section is the same as the exact Quantum Mechanical cross section even in the region where classical approximations do not hold. Therefore although the de Broglie wavelength criterion would limit the experiment to be performed for an

incident energy below 150 ev, this restriction can be ignored providing the scattering events are coulombic, and thus we assume 800 ev as an upper limit.

For a lower limit the restriction is placed that the incident particle energy should be greater than any of the binding energies of the systems involved. Thus a lower energy limit of about 25 ev should constitute a suitable value.

Therefore, between the limits of 25 and 800 ev there exists a region wherein the method of the impulse approximation using classical theory is valid.

(b) Wire Orbit Method

This method (1960, 1956a) is based on the equivalence relating the path of a flexible wire carrying an electric current in a magnetic field, and the trajectory of a charged particle passing through the same field.

Consider a small length ds of flexible wire carrying a current and under a tension in a magnetic field as shown in Fig. 2. Using Gaussian units, we let

$\vec{n}$ = unit vector normal to current carrying wire

$\frac{\vec{n}}{\rho}$ = curvature of wire (directed away from the center)

$\vec{t}$ = unit vector tangent to wire and in direction of current

i_a = current in abamperes

$\vec{T}$ = tension of wire in dynes

$m_w\vec{g}$ = weight per unit length of wire in dynes/cm

$\vec{B}$ = magnetic flux density vector in gauss

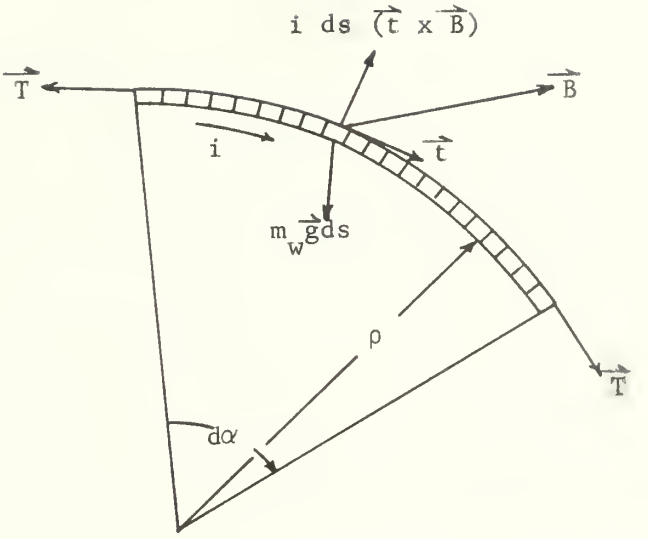

Fig. 2

Forces on a Small Segment of a Current-Carrying Wire in a Magnetic Field

It can be seen that $\vec{t}$, $\vec{n}$, and $\vec{T}$ are coplanar, and at equilibrium the sum of the magnetic force, the gravitational force, and the tension must equal zero, giving

$$i_a ds\ (\vec{t} \times \vec{B}) - 2T \frac{d\alpha}{2} \vec{n} - m_w \vec{g} ds = 0 \qquad (21)$$

Letting $ds = \rho d\alpha$, we have (22)

$$i_a ds\ (\vec{t} \times \vec{B}) - T \frac{ds}{\rho} \vec{n} - m_w \vec{g} ds = 0 \qquad (23)$$

from which the curvature of the wire is obtained in the following form

$$\frac{\vec{n}}{\rho} = \frac{i_a}{T} (\vec{t} \times \vec{B}) - \frac{m_w \vec{g}}{T} \quad . \qquad (24)$$

A similar expression may be obtained for the path of a charged particle in the same field. We let

$\frac{\vec{n}}{\rho}$ = curvature of particle trajectory

$\vec{t}$ = unit vector tangent to trajectory and in direction of velocity

$\frac{e}{pc}$ = charge to momentum ratio of particle in gaussian units

The differential equation for the path of the particle is described by

$$\frac{d\vec{p}}{dt} = \frac{e}{c} (\vec{v} \times \vec{B}) \quad . \qquad (25)$$

Now

$$\vec{t} = \frac{\vec{p}}{p} = \frac{\vec{v}}{v} \quad \text{and} \quad ds = vdt \qquad (26)$$

therefore

$$\frac{vd\vec{p}}{ds} = vp \frac{d\vec{t}}{ds} = \frac{ev}{c} (\vec{t} \times \vec{B}) \qquad (27)$$

but

$$\frac{d\vec{t}}{ds} = \frac{\vec{n}}{\rho} \tag{28}$$

and the curvature of the path is

$$\frac{\vec{n}}{\rho} = \frac{e}{pc} (\vec{t} \times \vec{B}) \ . \tag{29}$$

If the weight of the wire can be neglected[1], then the curvature equations (24) and (29) are identical when

$$\frac{T}{i_a} = \frac{pc}{e} \tag{30}$$

and the wire and the particle path will coincide for equal boundary conditions (end points).

It is convenient to express equation (30) in experimentally useable units. We take the charged particle as the scattered H_2^+, e as a unit positive charge, and convert the momentum p to its energy equivalent by the expression

$$E = \frac{p^2}{2m} \ . \tag{31}$$

Because of different velocities, the energy of the incoming proton is equal to the scattered H_2^+ particle. Therefore, using the appropriate conversion units,we have for the expression relating the wire and particle paths

$$E^{\frac{1}{2}} = 48 \frac{M}{i}$$

1. A rough calculation made on an average trajectory shows that the ratio of the magnetic to the gravitational force is of the order of about 100.

where E is the energy of incoming protons in units of electron volts, M is the tension of the wire in grams, and i the wire current in amperes.

3. Magnetic Field Measurements

(a) Experimental Equipment

1. Magnet Coil

The magnet coil (1956c) consists of a set of five concentric brass spools wound with number 14 copper wire. For adequate cooling 1/4 inch o.d. copper tubing is placed at the outer layer of each spool. The individual cooling coils are connected to a common manifold and then to a cold water supply. Fig. 3 shows the electrical circuit of the five layers arranged to distribute the resistances as evenly as possible. A rough estimate of the maximum safe coil current indicated a value in the neighborhood of 15-16 amperes.

2. Power Supply

In order to fulfill the specifications of an output current of 0-15 amperes and a regulation of about $\pm$ 0.1% to include both line fluctuation and voltage ripple, a Sorensen Nobatron model DCR 150-15 power supply was acquired and found to satisfactory.

3. Hall Axial Probe

As the axial component of the magnetic field predominates in the area in which we are interested, it was sufficient only to measure this component. The principal problem faced in the measurement of the field was that of accurately positioning the measuring equipment within the long aluminum tube concentric with the axis of the magnetic coil. Conventional gaussmeters or nuclear resonance probes could not be inserted into the tube at the desired positions. To overcome the above problem, a Halltron HP-315 Axial Field Hall probe[1] was used. The probe

1. Ohio Semitronics, Inc., 1205 Chesapeake Avenue, Columbus, Ohio.

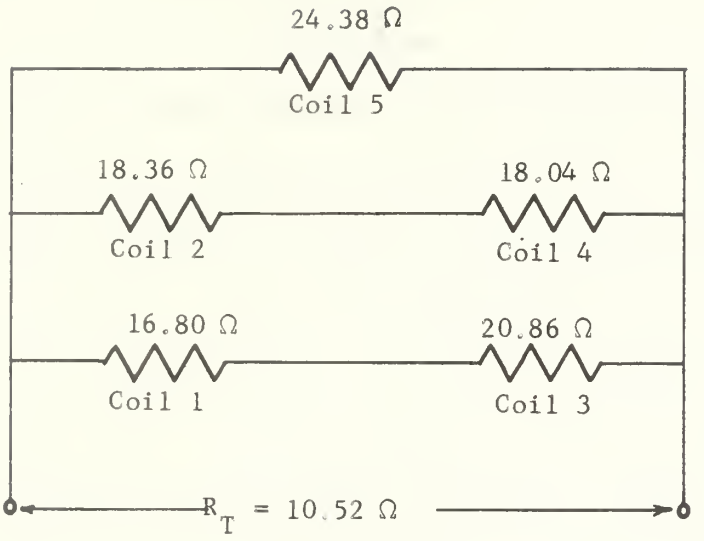

Fig. 3

Circuitry of Magnetic Coil

(Coils 1 through 5 are labeled from inner to outer layer respectively. Resistances are measured in ohms.)

itself was placed in a plastic capsule with a long 4-wire cable attached to the input and output terminals of the probe. Attached to the forward tip of the probe was the positioning device consisting of a wooden rule accurate to within 1 mm.

To provide accurate positioning, a 3/4 inch aluminum pipe was fitted through two templates as shown in Fig. 4. Cross hairs were scribed onto the templates to allow for azimuthal alignment with a carpenter's level. Seven 3/4 inch holes were cut, 1/2 inch apart on an axis radially from center, to provide for the positioning of seven radial measurements for each azimuthal setting of the templates.

The encapsulated probe was calibrated in a variable magnetic field against a known nuclear magnetic resonance (NMR) probe accurate at 1000 gauss to ± 1 gauss. Magnetic field values were calculated for proton resonance in water from the expression:

$$H(\text{kilogauss}) = \frac{\nu}{4.2577} \quad (\text{resonant frequency in mc/sec}) \qquad (32)$$

The circuitry consisted basically of steady 100 milliampere current fed into the probe with probe output voltages being read across a four ohm resistor with a potentiometer readable to $\pm .05$ millivolts. Nine calibration points were fed into a "least square" curve fitting program on the CDC 1604 computer, and a first degree polynomial was found to give the best fit.

(b) Measurements and Results

The probe system was assembled and mounted on the aluminum tube. The initial run consisted of measurements taken 4 cm apart along

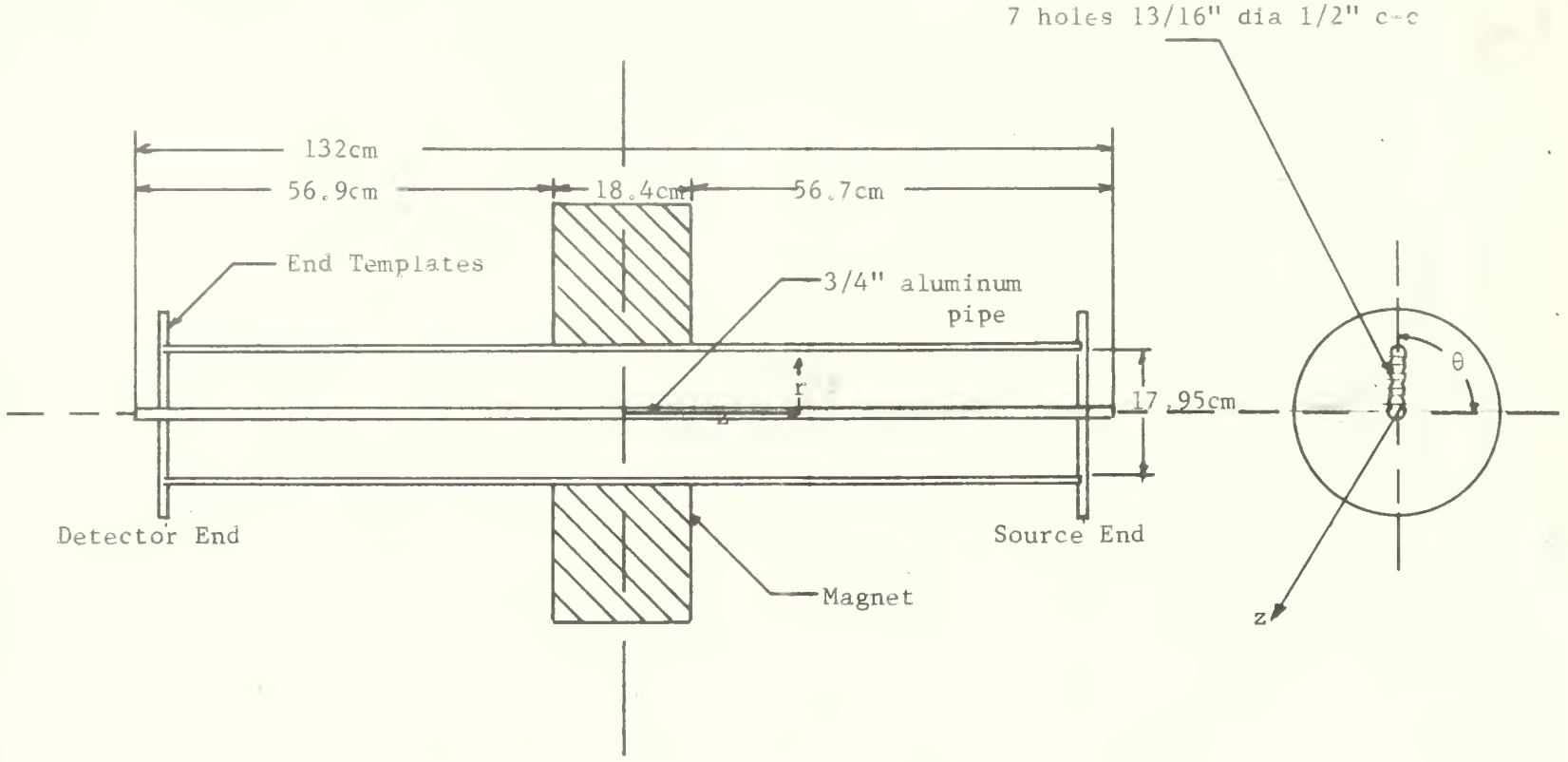

Fig. 4

Positioning of Hall Probe

the axis of the magnet at current settings of 2, 4, 6, 8, 10, 12, and 14 amperes respectively. The complete tabulation of these values is to be found in Appendix 1, Table I. A plot of the field strength, taken for the above current settings and at fixed locations (z = 0, 14, 42) along the magnet axis, is shown in Fig. 5. It can be seen that the field strength is linear over the complete range of magnet current settings. Plotting the field strength along the axis of the magnet for four different current settings (Fig. 6) indicates the symmetry of the field along the axis and shows its largest values located at or near the z = 0 plane (the center of the magnet).

In order to determine the axial component of the magnetic field at points off the axis, another series of measurements were made in the vertical planes defined by $z = 0$, $z = \pm 14$, $z = \pm 42$ cm at 1/2 inch radial intervals, and at every 45 degrees from 0 to 360. The results of these measurements are tabulated in Appendix 1, Table II, and plotted in Figs. 1-1 through 1-5. It can be seen that for a given radial dimension, the field is azimuthally relatively symmetric. At the center of the magnet its strength increases radially approximately 10 percent, at 14 cm from the center it decreases radially some 7-8 percent, and at the ends it is constant.

Upon completion of the magnetic field measurements, the aluminum tube was removed as it was not needed for the trajectory work.

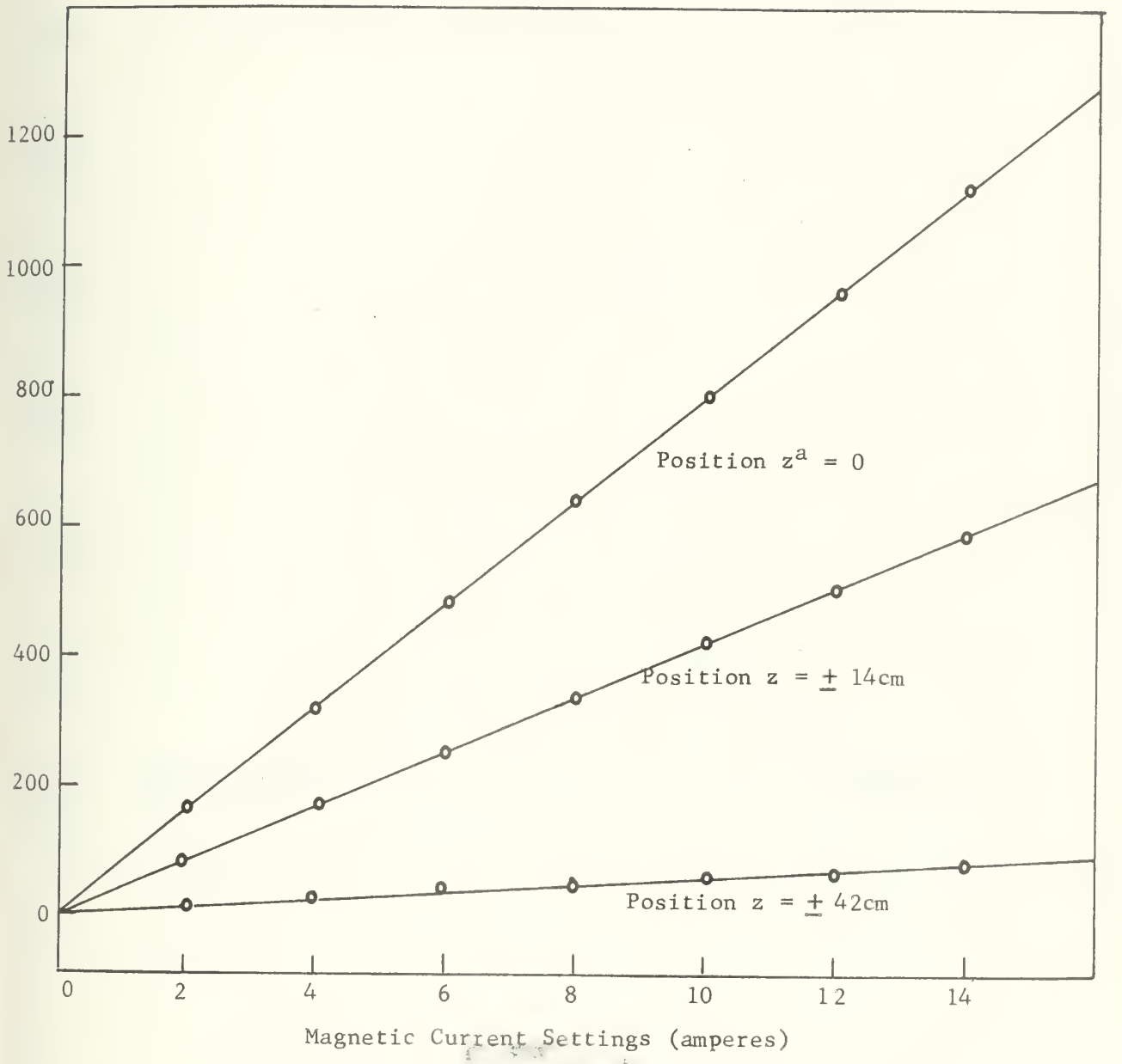

Fig. 5

Axial Component of Magnetic Field Strength as Function of Magnet Current at Various Positions along Magnet Axis

a. See Fig. 4 for interpretation.

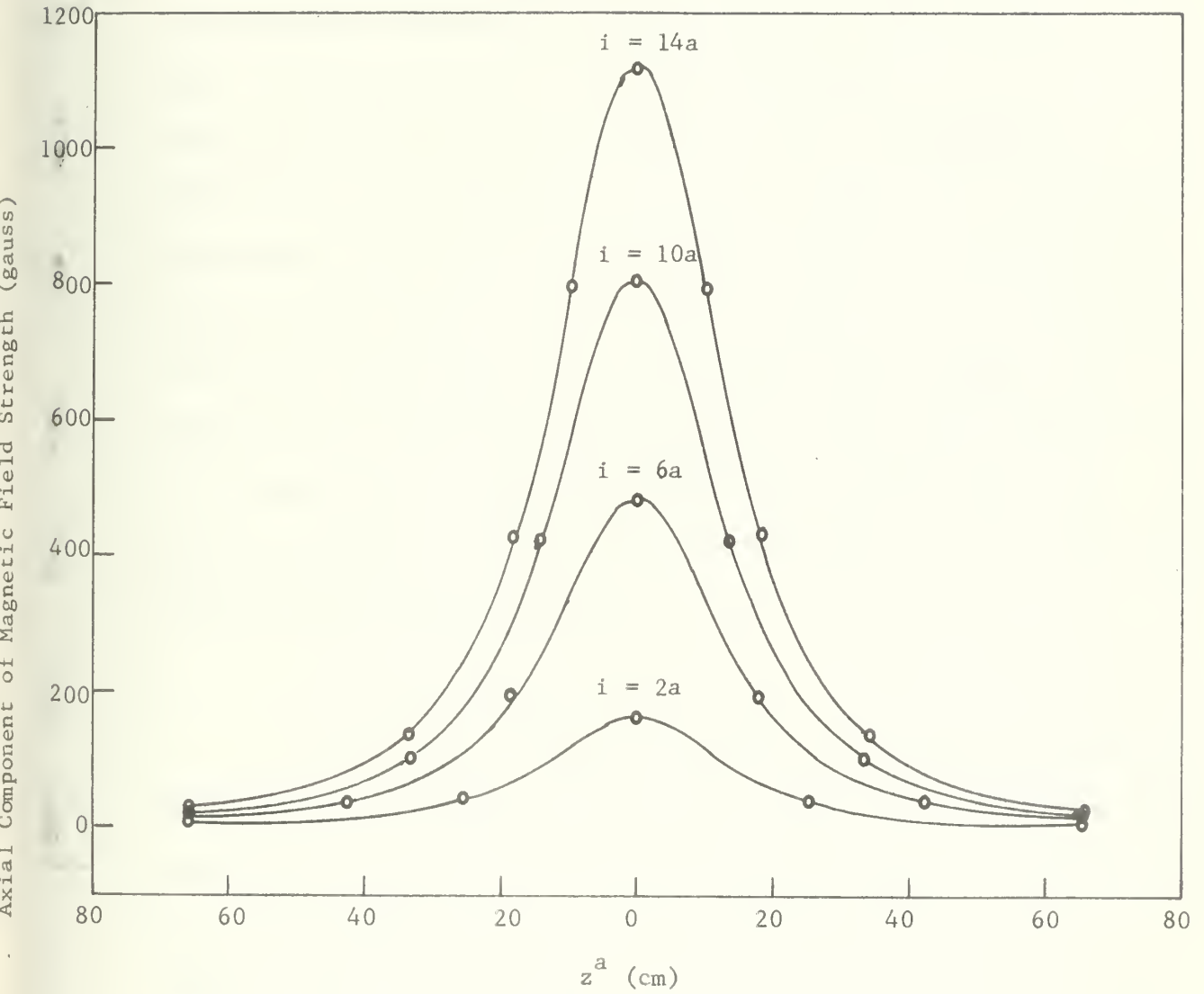

Fig. 6

Axial Component of Magnetic Field Strength along Axis
for Various Magnet Current Settings

a. See Fig. 4 for interpretation of z

4. Particle Trajectory Measurements

(a) Experimental Equipment and Arrangement

1. Establishing Magnet Axis

The use of symmetry suggested that the scattered particles of the proposed experiment should both leave and refocus on the magnet axis. This dictated that all the measuring equipment used in the wire orbit method should be positioned on this axis. Four equidistant indentations were scratched into the flange of each side of the magnet. Thin strings were stretched across opposite indentations establishing two known points along the magnet axis. A surveying transit was placed in line with these points some 230 cm distant from the magnet. This instrument was selected over a string line or other optical devices as it is located outside the orbit area and does not block any of the measuring equipment. Rechecking the transit before each run insured that all measuring equipment was on line.

2. Current Carrying Wire

Drawing from the experience gained at the Lawrence Radiation Laboratory of the University of California (1956b), an uninsulated wire[1] consisting of 14 strands of #44 copper wire was used. It weighed approximately .08 grams/ft which produced some sag in the trajectory, but not enough to cause an appreciable error in the measurements. It was found that it could safely take any current up to 4.5 amperes, but that at higher currents it would become oxidized and less flexible.

A few strands of this wire also produced an excellent trajectory, but because of the low currents and tensions involved, this wire was not used.

---

1. Purchased from New England Electric Works, Inc., 367 Main Street, Lisbon, New Hampshire.

3. Angle Measuring Instrument

To measure the departure angles of the wire, the measuring instrument shown in Fig. 7 was constructed. A copper sleeve was made to turn on a one inch o.d. plastic pipe. The sleeve protruded over the pipe forming an angle with the pipe axis on which angles from 35 to 55 degrees were scribed in one degree increments in an arrangement similar to that of a micrometer. Those readings which fell between the scribed angles were found through interpolation. At the end of the plastic pipe a 3/32" o.d. teflon ball was placed on axis and designed to rotate in any direction. The wire passed through the pipe and through a small hole in the ball and was secured to the rear of the ball by a simple knot. A galvanometer was hooked up to the sleeve and indicated contact whenever the sleeve touched the current carrying wire. The pipe with its attached sleeve was centered inside the core of the magnet along the axis as shown in the schematic of Fig. 8.

A run of fifteen measurements taken for the same angle indicated a value accurate to about $\pm$30 minutes. Due to the curvature of the wire leaving the device, the particle departure angle as measured θ_m does not exactly reflect the correct particle departure angle θ_c. An expression relating these two angles is derived in Appendix 2 in the form of the following transcendental equation:

$$R\, f \csc \theta_c = \sin (f\, R \cot \theta_m \sec \theta_c) \qquad (33)$$

where R is the radius of the copper conductor sleeve and f is a function of the magnetic field strength and the particle momentum. A computer program was written for this expression, with the results indicating an additive correction of 30 minutes or less.

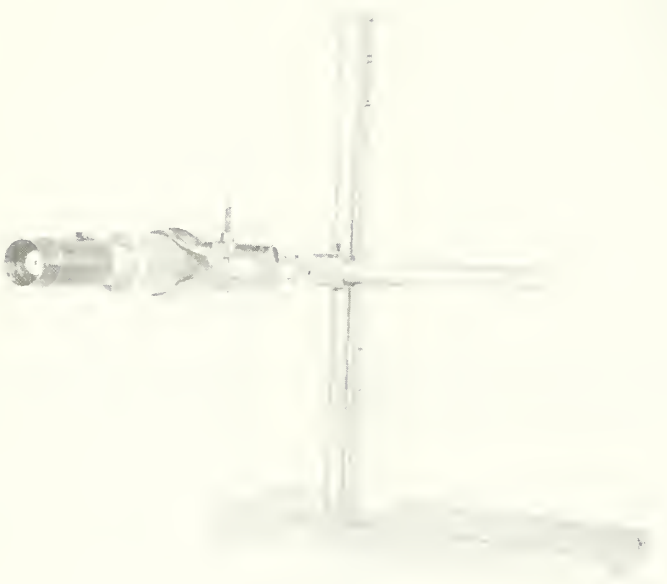

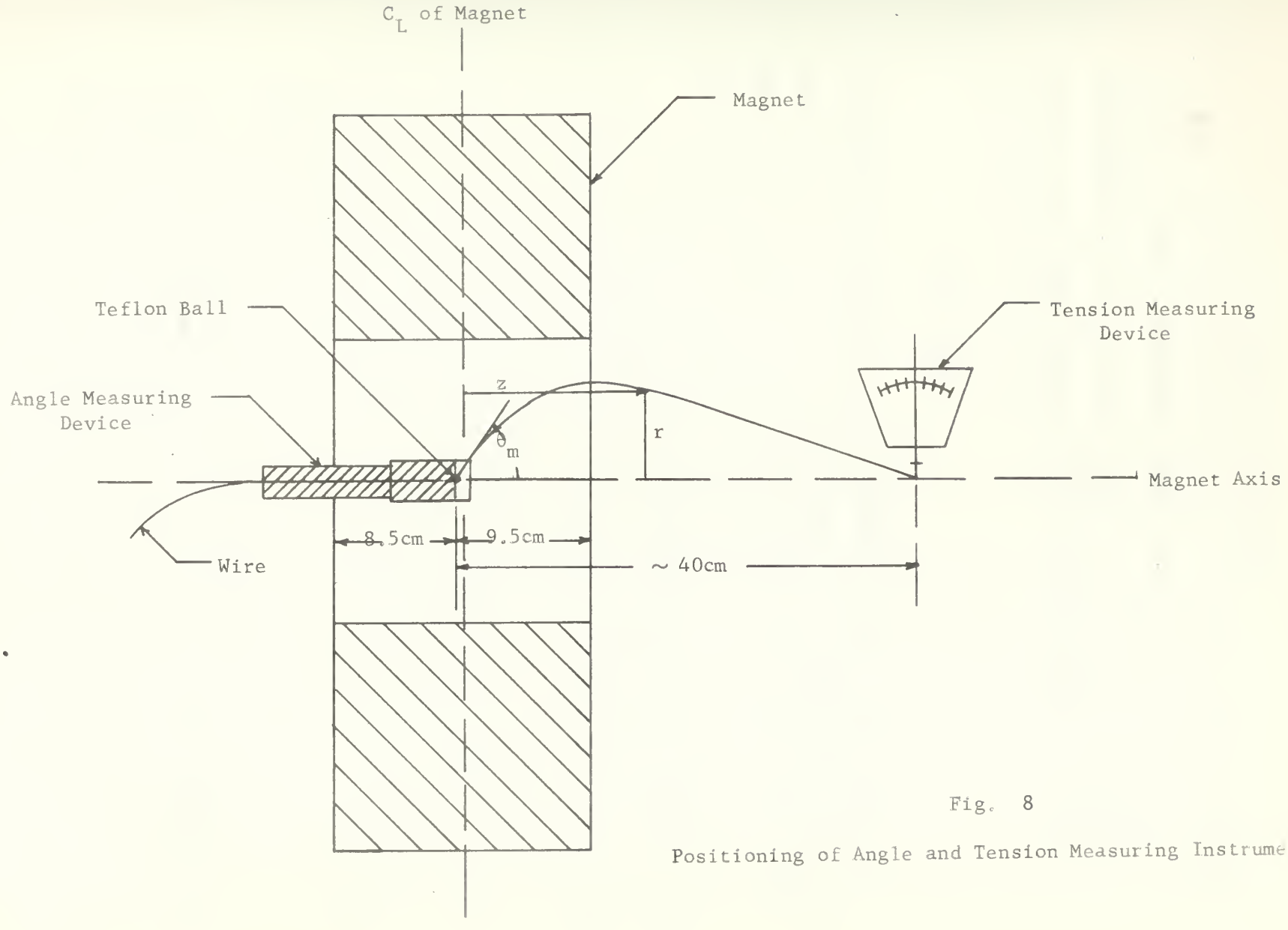

Fig. 8

Positioning of Angle and Tension Measuring Instruments

4. Tension Measuring Instrument

One of the objectives of this experiment was to find $\left(\frac{d\theta}{dB}\right)_E$, the rate of change of particle departure angle with respect to the magnetic field at constant energy. A pulley was the immediate answer as any weight hanging over it would have kept the ratio of M/i constant in the expression

$$E^{\frac{1}{2}} = 48 \frac{M}{i}$$

independent of manipulation of the magnetic field. Much effort was expended into devising a suitable pulley, all of which met with failure due to the fact that the inherent friction of the pulley could neither be eliminated nor reduced.

As a result of not finding an adequate pulley, the instrument shown in Fig. 9 was constructed to measure the tension in the wire. It consisted basically of a 4 inch brass-bronze wire shaped in the form of an "L" which followed the principle of a leaf spring. One end was held rigid, and the other end contained the flexible wire clamped to it by a small teflon wedge. The bar of the "L" was placed in contact with the bottom of a pointer of an ammeter scale cut down for this purpose. Any deflection of the wire spring caused a corresponding deflection on the scale pointer.

This instrument was calibrated by turning it on its side and hanging known weights from it. A further check of the calibration was made by placing the instrument in its normal upright position and using a pulley with the same weights. The calibration curve is shown in Fig. 10.

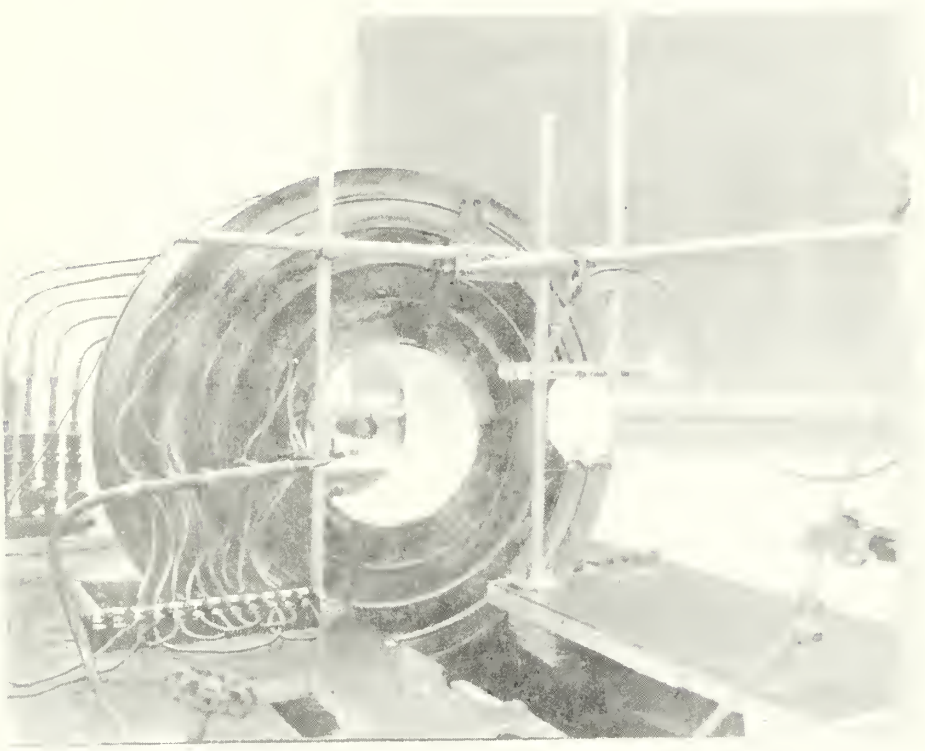

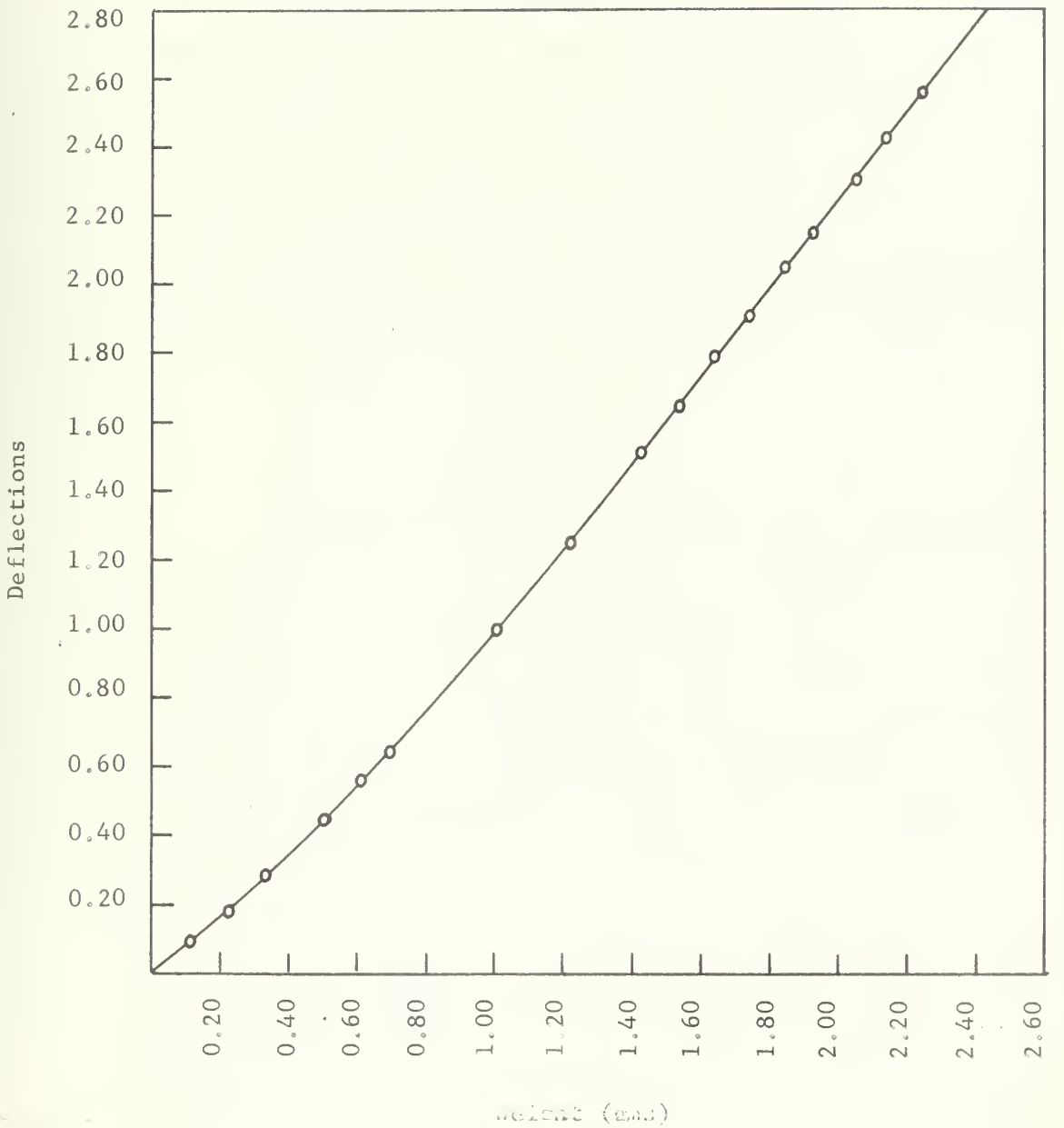

Fig. 10

Calibration Plot of Tension Measuring Instrument

It must be realized that this method of measuring the tension had two distinct disadvantages over that of the pulley. First and most important of all, there was no way of keeping the tension, and thus the energy, constant as one changed the magnetic field. This meant that much data would have to be taken and the partial derivative of $\left(\frac{d\theta}{dB}\right)_E$ could even then only be found indirectly. In addition, as the wire spring was displaced, the location where the flexible wire focussed back on the magnet axis also moved. This was not too serious as the angle of acceptance for the detector to be eventually placed at this position is more than large enough to cover this variance.

5. Orbit Measuring Instrument

To measure a point on the orbit of the wire we were interested in two dimensions; its axial distance z from where the wire left the angle measuring instrument, and its radial distance r from the axis, as shown in Fig. 8. A simple but extremely functional device (Fig. 11) was built to do this. A metric tape was placed parallel to but below the magnet axis and referenced to the center of the magnet. A slide with an attached pointer was located on a long aluminum angle bar. Supported above the slide was an arm, containing the radial measuring device on one end, exactly positioned on the magnet axis. A screw on the radial measuring device controlled a brass ruler calibrated in mm which could be extended until it just touched the flexible wire. The parts of this device as well as all other measuring instruments were constructed of non-magnetic materials.

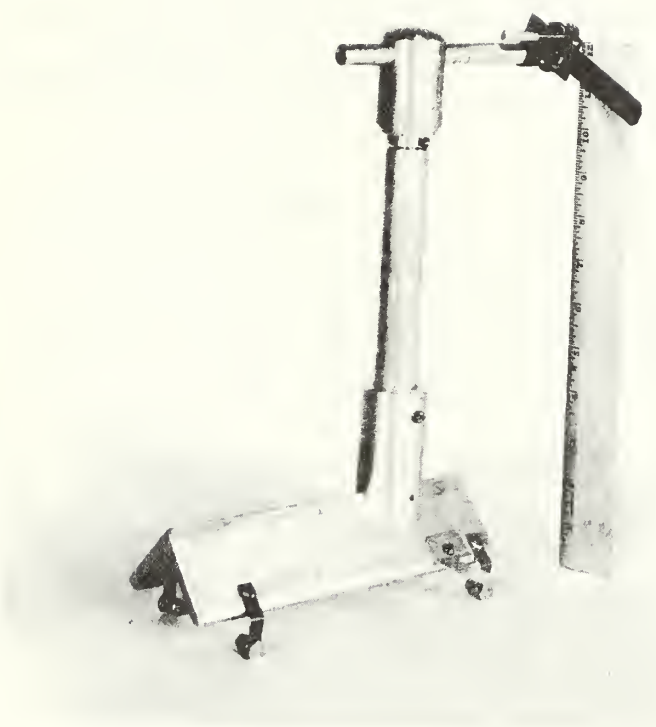

Fig. 11

Orbit Measuring Device

6. Positioning of Measuring Equipment

It was experimentally determined that the best wire trajectory occurred if the angle measuring instrument was placed on the magnet axis with the wire departing near the center of the magnet where the field has its greatest strength. In this position the wire could depart at any angle between 35 and 55 degrees. The tension measuring device was positioned approximately 40 cm down axis from this point as shown in Fig. 8. A closer positioning would cause the wire to touch the sides of the magnet for large departure angles, and for a more distant position, the wire would have too much sag. Fig. 12 shows the wire trajectory and all measuring equipment in place.

(b) Results and Discussion

1. Existence of a Unique Trajectory

Consider a charged particle leaving a point in a uniform magnetic field with its initial velocity vector at an angle θ_c with respect to B . This particle will describe a helical trajectory and return to the original field line a distance L from its starting point. It is shown in Appendix 3 that the following relationship holds.

$$LB = KE^{\frac{1}{2}} \cos \theta_c \qquad (34)$$

where L = axial distance travelled in one revolution

B = magnetic field strength

K = constant

E = particle energy

θ_c = departure angle

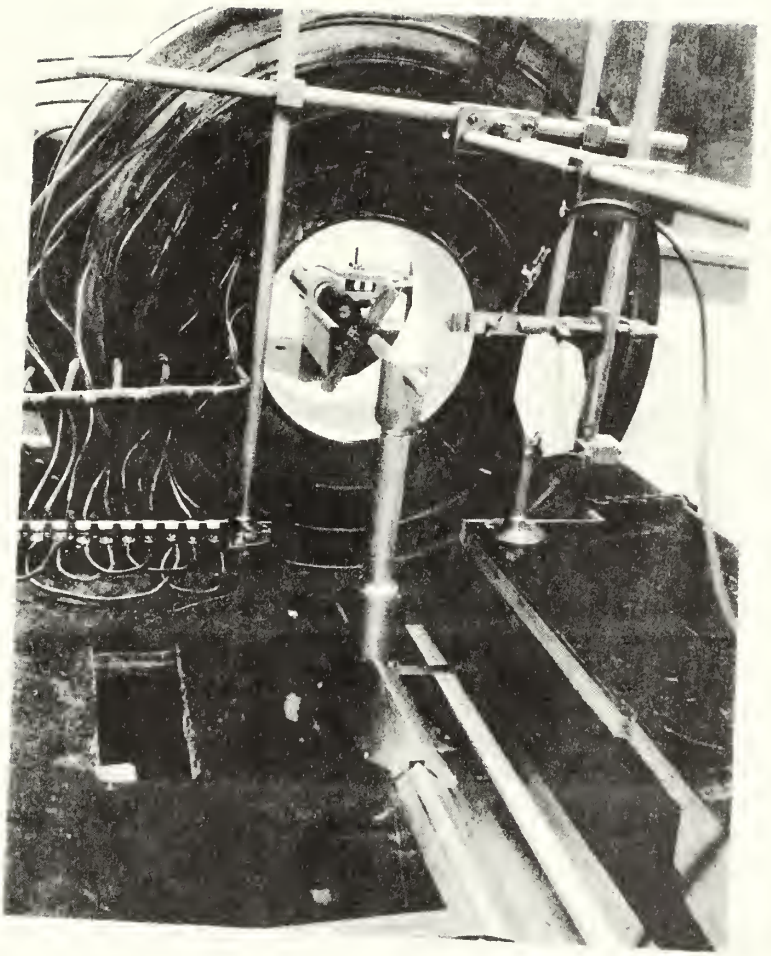

Plate 12

All Wire Orbit Measuring Devices in Place

Equation (34) shows that for given values of L, E, B and θ_c there exists a unique trajectory, since both the force on the particle and the initial conditions are completely fixed by (34).

Since it is not possible to write down the corresponding expression for the case of non-uniform fields, a qualitative experimental test was carried out as follows:

Keeping the field current and the length along the axis between measuring instruments constant, but varying the actual length of wire, it was noticed that both the equivalent particle energy and the departure angle changed. This experiment was performed several times, and with each trial a different trajectory was produced. It seems then that there is indeed a unique trajectory when the parameters θ_c, B, L, and E are specified.

2. Particle Trajectory Measurements

It was originally hoped that in the collision experiment one could analyze the angular distribution of the scattered particles leaving at a given energy by using baffles and by adjusting the magnetic field to examine a narrow angular spread at a particular angle. To determine the feasibility of this idea, the wire orbit method was utilized.

The first objective was to examine the actual particle trajectories for different values of departure angle, particle energy, and magnet current. A complete tabulation of this data is to be found in Appendix 4. In order to have some feeling for the general shape of these trajectories, two plots have been made. Fig. 13 shows two trajectories for approximately equal particle energies but at different angles, while Fig. 14

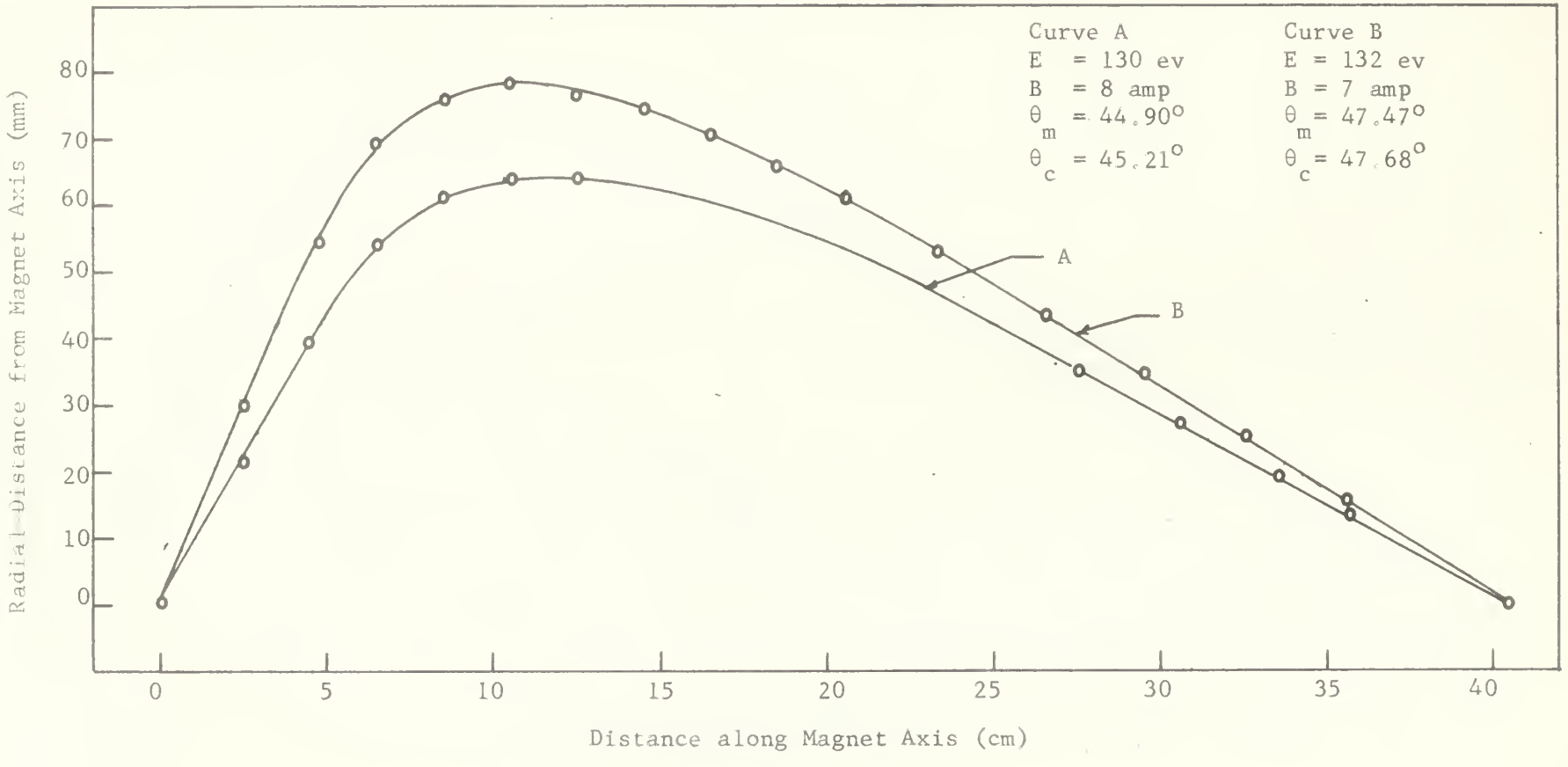

Fig. 13

Plot of Particle Trajectories for Approximately Equal Particle Energies

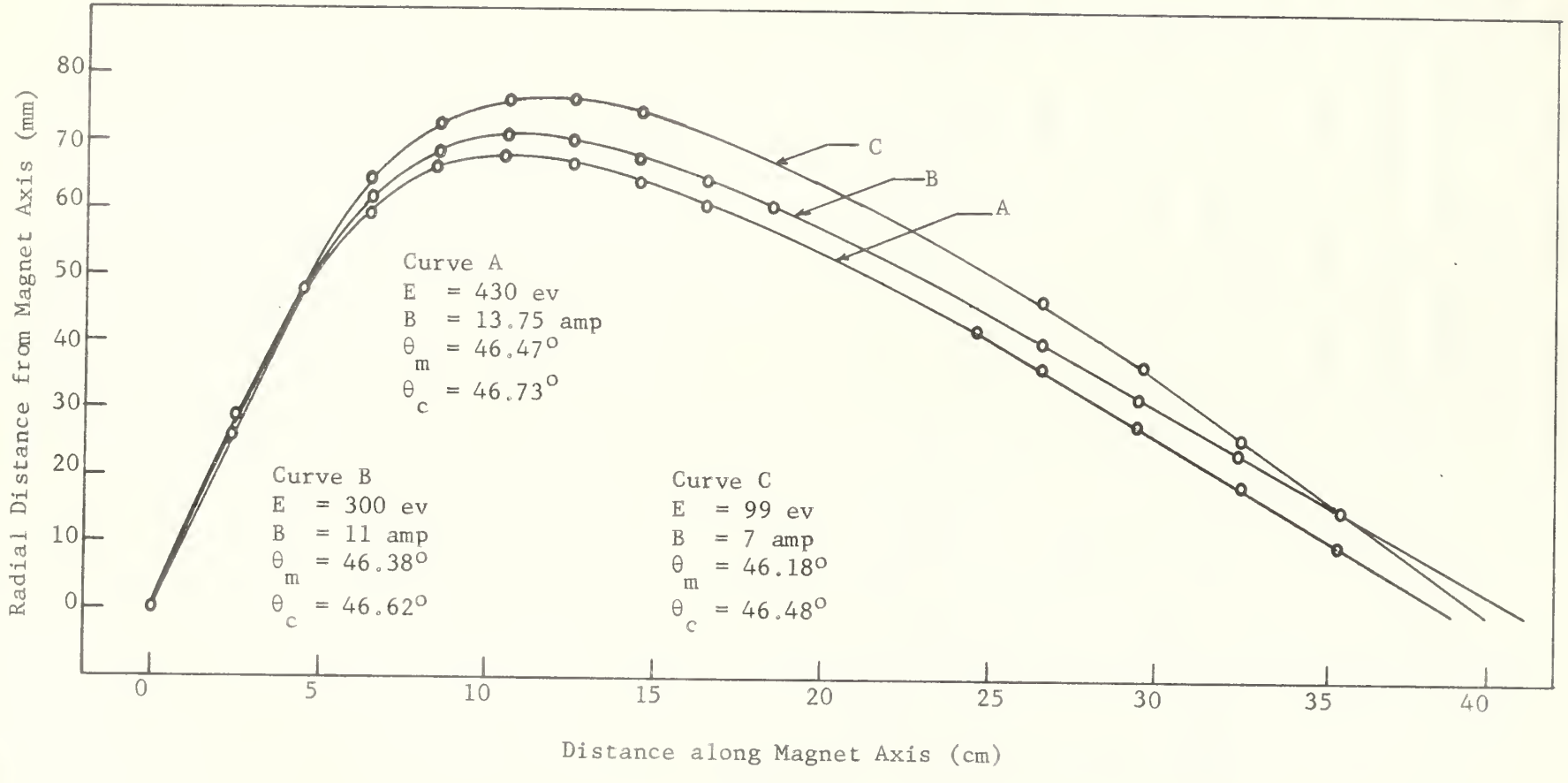

Fig. 14

Plot of Particle Trajectories for Approximately Equal Departure Angles

shows three trajectories for approximately equal angles but at different particle energies. Although the actual trajectory follows the path of a spiral, only the radial distance of the trajectory from the magnet axis has been plotted. Note that each trajectory starts off linearly, reaches a maximum curvature between 9 and 14 cm from its initial departure point, and then returns linearly to the axis.

In the second objective, we were interested in determining the rate of change of particle departure angle with respect to the magnet current while holding the particle energy constant. This data is tabulated in Table I and plotted in Fig. 15. Because this data had to be obtained indirectly, it is somewhat less reliable than the directly measured quantities. However, in the 200-500 ev range the value of $\left(\frac{d\theta}{dI_B}\right)_E$ seems quite consistent and has a value of about 3^o/amp.

Table I

Calculation of Rate of Change of Particle Departure Angle with Respect to Magnet Current at Constant Energy

Corrected angle[a] of departure (degrees)	Particle Energy (ev)	Magnet Current (amp)	$\left(\frac{d\theta}{dI_B}\right)_E$ (degrees/amp)
52.74	108	7	10.09
42.65	108	8	
48.12	133	8	9.37
38.75	137	9	
45.44	193	9	3.59
41.85	193	10	
45.80	338	11	2.68
43.12	332	12	
45.95	440	12	2.85
43.10	445	13	
47.09	630	13	0.76
46.52	640	13.75	

a. All angles are accurate to $\pm$ 0.50 degrees.

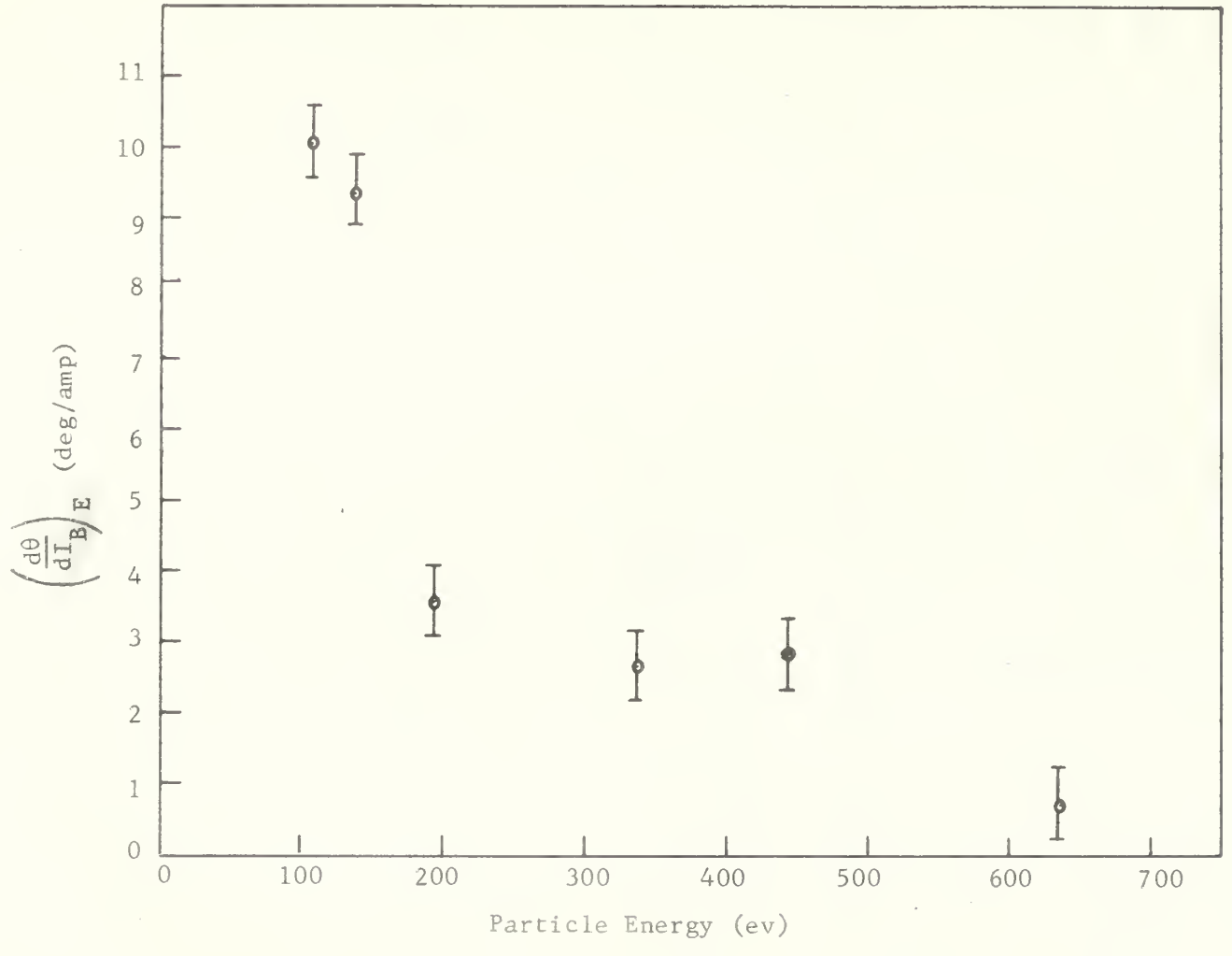

Fig. 15

Rate of Change of Particle Departure Angle with Respect to Magnet Current at Constant Energy

5. Conclusion

Through the wire orbit method it has been shown that by using the existing magnet, it is indeed possible to obtain H_2^+ trajectories in the required energy range of 25-800 ev having departure angles between 35 and 55 degrees. For the above energy and angular requirements, it was experimentally found that one set of trajectories exists which depart near the center of the magnet and return to the axis approximately 40 cm away. Although valid trajectories may exist for other end point positions, time did not permit these to be investigated.

From Figs. 13 and 14, one concludes that for fixed initial and end points, the trajectories are very similar to each other. This would seem to make the use of baffles as a particle trajectory discriminating mechanism very doubtful.

Typical values of the rate of change of departure angle with respect to magnet current at constant energy $\left(\frac{d\theta}{dI_B}\right)_E$ were found to be of the order of 3 deg/amp in the energy range of 200-500 ev.

It is expected then that the technique to be utilized for differentiating particles emerging with different departure angles at a given energy will involve both moving the detector along the axis and varying the magnet current. This paper has shown that both these methods can be used and the numerical analysis presently being conducted should produce the necessary quantitative information needed.

Finally, it is shown that if the particle energy, departure angle, magnetic field, and the distance between the initial and end points of the trajectory are fixed, there exists a unique trajectory.

6. Acknowledgements

It is with deep appreciation and gratitude the I acknowledge the support and encouragement of Dr. Otto Heinz of the Naval Postgraduate School faculty at whose suggestion this project was undertaken. I wish to thank Dr. C. J. Cook of Stanford Research Institute for his assistance in further explaining the Impulse Approximation. Professor S. H. Kalmbach of the School faculty suggested the method used for the angle measurements along with several other valuable ideas. Dr. W. Judd and Mr. J. H. Dorst of the Lawrence Radiation Laboratory contributed much of their knowledge and experience of the wire orbit method. I am indebted to Mr. M. K. Andrews, the Physics Department instrument maker, whose efforts and talents in constructing all the measuring equipment made this project possible. I also wish to thank Mr. Robert Moeller and Mr. Tom Maris, also the the School technical staff, for all the assistance rendered by them. Finally, I am grateful to Miss Sharon Raney of the School Computer Facility for writing the program to compute the correct particle departure angles.

7. Bibliography

1951 Bohm, D., Quantum Theory, Prentice Hall, 1951

1956a Lambertson, G. R., "Use of the Wire Loop in Locating the Orbital Surface of a Cyclotron Field", UCRL-3366, 1956

1956b Lambertson, G. R., "Tests of a Flexible Wire for Particle Trajectory Studies", UCRL, UCID 647, MT-41A, 1956

1956c Rosell, F. E., Thin Lens Beta Spectrometer, Thesis (M.S.), USNPS, Monterey, California, 1956

1960 Chamberlain, O., "Optics of High Energy Beams", Amer. Rev. Nuclear Sci., 10, 161, 1960

1964a Bates, D. R., Cook, C. J., and Smith, F. J., "Classical Theory of Ion-Molecule Rearrangement Collisions at High Impact Energies", Proc. Phys. Soc. (London), 83, 49, 1964

1964b McDaniel, E. W., Collision Phenomena in Ionized Gases, Wiley, 1964

Appendix I

Table I

Axial Magnetic Field Strength along Axis of Magnet for Various Currents

Distance along Axis from Center of Magnet (cm)	Magnetic Field Strength (gauss)						
	I = 2	4	6	8	10	12	14 amp
z^a = 66	7	12	16	18	23	28	30
62	9	14	18	21	25	30	37
58	10	16	20	25	31	38	42
54	10	18	23	31	36	43	47
50	12	20	29	34	43	49	57
46	14	23	32	43	53	59	69
42	16	29	40	53	64	72	85
38	20	34	49	65	80	92	105
34	25	43	62	84	100	119	137
30	31	56	82	108	131	152	176
26	40	73	106	141	172	203	234
22	51	95	142	186	232	269	313
18	67	128	190	254	315	373	430
14	89	172	258	342	429	502	590
10	117	229	342	454	568	675	795
6	144	284	425	564	704	843	985
2	163	319	478	634	793	945	1110
0	164	322	484	641	805	958	1125
- 2	163	319	478	632	793	945	1110
- 6	144	284	421	562	700	843	985
-10	117	227	341	454	564	675	795
-14	89	172	256	341	427	502	590
-18	67	128	190	252	311	373	430
-22	51	93	141	186	230	269	313
-26	38	71	104	139	172	203	234
-30	29	54	82	108	131	152	176
-34	23	43	62	84	100	119	137
-38	18	34	49	64	80	92	105
-42	16	27	40	53	64	72	84
-46	14	23	32	43	53	59	69
-50	12	20	27	36	43	49	57
-54	10	18	25	31	36	43	47
-58	10	16	20	27	31	38	42
-62	9	14	18	21	27	30	37
-66 (Detector End)	7	12	16	18	25	28	30

a. See Fig. 4 for orientation of coordinate system.

Appendix I

Table II[c]

Axial Magnetic Field Strength off Axis of Magnet

Distance along Axis from Center of Magnet (cm)	Radial Distance from Magnet Axis (cm)	Magnetic Field Strength[a] (gauss)							
		θ^b = 0	45	90	135	180	225	270	315°
z^b = 42	r^b = 0.00	62	64	64	62	62	64	64	62
	1.27	62	64	64	62	62	62	64	62
	2.54	62	64	62	62	62	64	62	62
	3.81	62	62	62	62	62	64	62	62
	5.08	62	62	62	62	62	62	62	62
	6.35	62	62	62	62	60	62	62	62
	7.62	62	62	62	62	60	62	62	60
z = 14	r = 0.00	427	429	429	429	429	429	429	429
	1.27	425	427	427	427	429	429	429	429
	2.54	421	421	425	425	427	429	427	427
	3.81	418	418	419	419	427	423	423	419
	5.08	412	412	412	414	421	421	419	410
	6.35	401	399	401	407	410	421	414	407
	7.62	396	385	388	394	399	405	403	399
z = 0	r = 0.00	801	801	805	803	803	805	803	803
	1.27	801	806	806	806	805	805	805	805
	2.54	806	808	806	810	810	814	806	814
	3.81	823	823	823	823	819	823	823	823
	5.08	843	843	843	843	841	843	838	843
	6.35	861	863	860	867	860	861	861	865
	7.62	889	891	887	893	887	894	887	896
z = -14	r = 0.00	427	425	427	427	427	427	425	427
	1.27	427	427	425	425	421	427	427	427
	2.54	425	427	421	421	418	423	419	423
	3.81	419	423	419	416	414	419	418	419
	5.08	414	418	414	410	405	410	408	410
	6.35	405	412	405	403	396	401	401	405
	7.62	394	403	397	394	385	388	388	390
z = -42	r = 0.00	64	64	64	62	62	64	64	62
	1.27	62	64	64	62	62	62	64	62
	2.54	64	64	64	62	62	64	64	62
	3.81	62	62	62	62	62	64	62	62
	5.08	62	62	62	62	62	62	62	62
	6.35	62	62	62	62	60	62	62	62
	7.62	62	62	62	62	60	62	62	60

a. All values of magnetic field strength were measured at a constant magnet current of 10 amperes.

b. See Fig. 4 for orientation of coordinate system.

c. Figs. 1-1 through 1-5 show this data plotted.

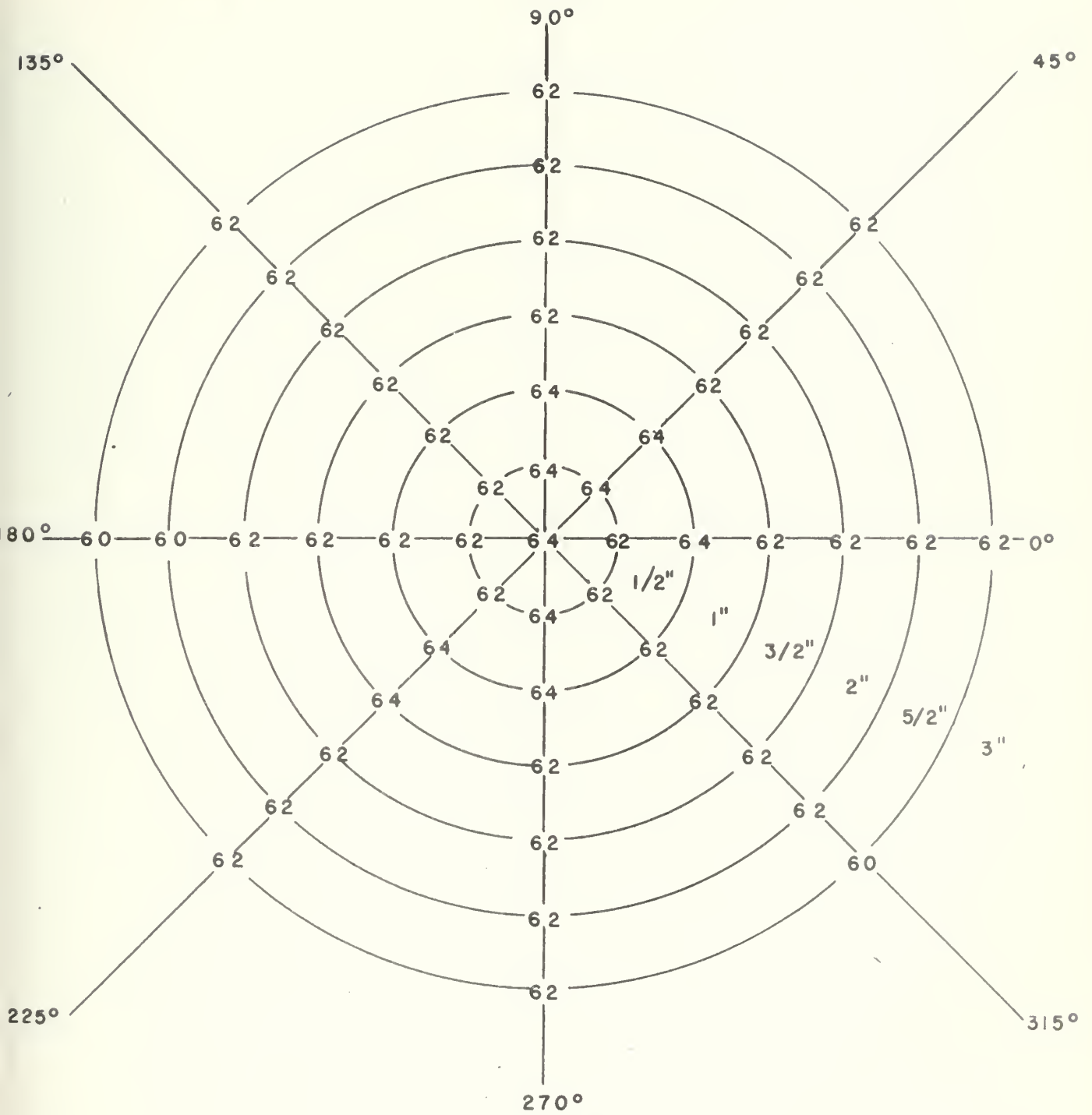

Fig. 1-4

(z = +42 cm)

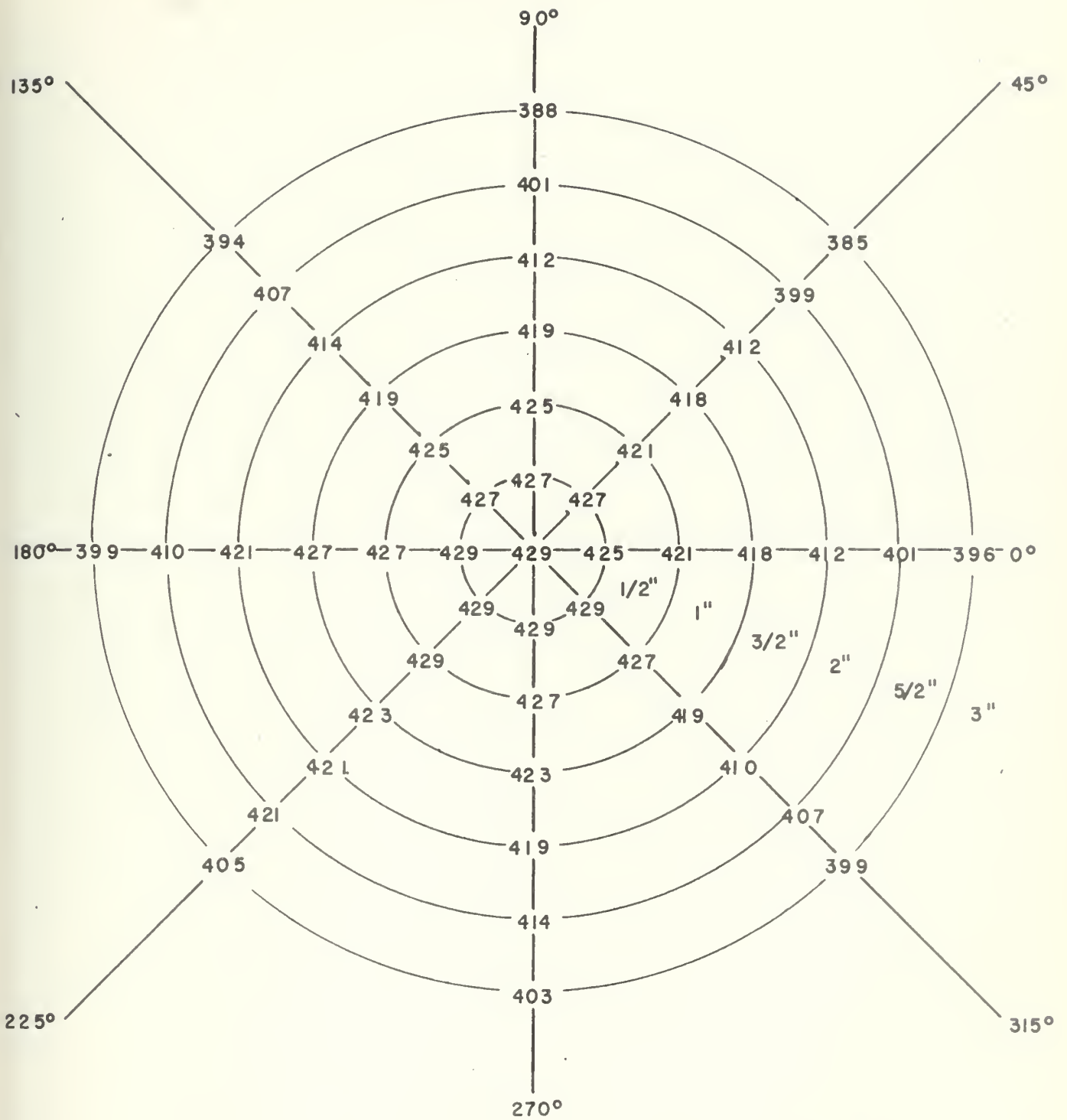
90°
135°
45°
388
401
394
385
412
407
399
419
414
412
425
419
418
425
421
427
427
427
180°
399
410
421
427
427
429
429
425
421
418
412
401
396
0°
1/2"
1"
3/2"
2"
5/2"
3"
429
429
429
429
427
427
423
419
421
423
410
421
407
419
405
399
414
403
225°
315°
270°

Fig. 1-2

(z = +14 cm)

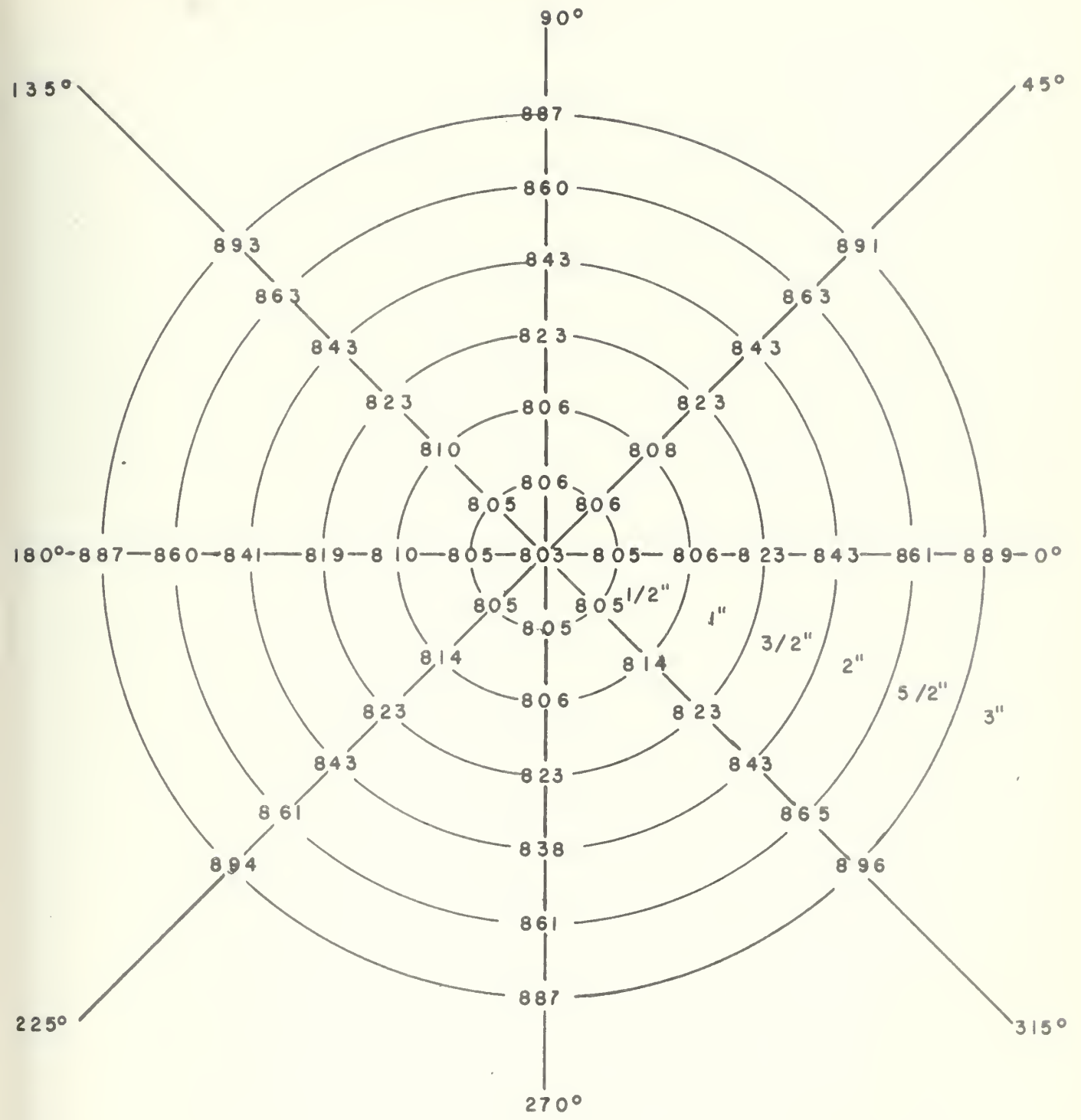
90°
135°
45°
887
860
893
891
843
863
863
843
823
843
823
806
823
810
808
806
805
806
180°-887—860—841—819—810—805—803—805—806—823—843—861—889—0°
805
805 1/2"
805
1"
3/2"
2"
5/2"
3"
814
814
806
823
823
843
843
823
861
865
838
894
896
861
887
225°
315°
270°

Fig. 1-3

(z = 0)

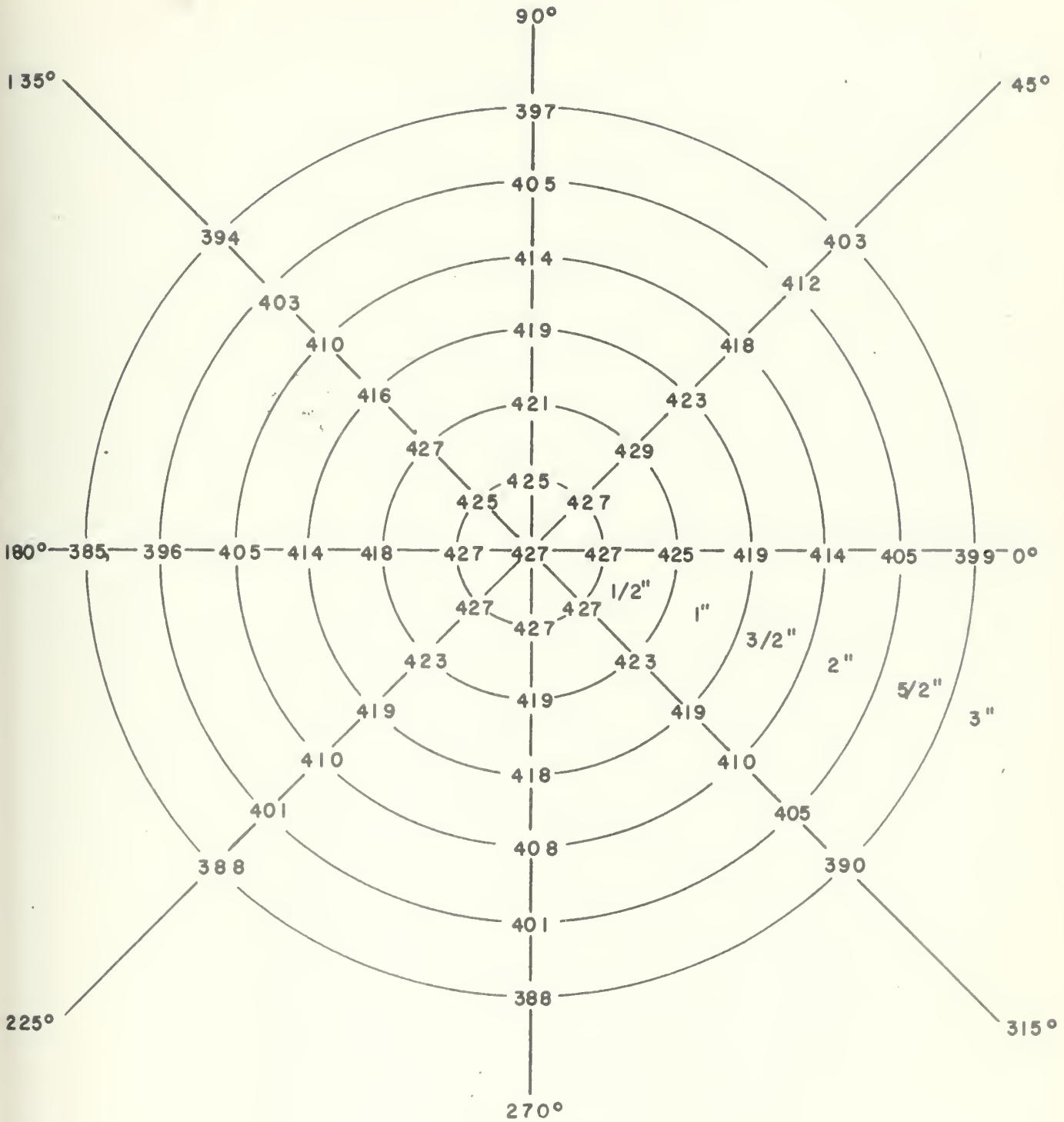
90°
135°
45°
180°
0°
225°
315°
270°
397
405
414
419
421
425
427
394
403
410
416
427
425
427
403
412
418
423
429
425
427
427
427
427
427
427
427
427
427
427
423
423
419
419
419
410
418
410
401
405
408
388
390
401
388
385
396
405
414
418
427
427
427
425
419
414
405
399
1/2"
1"
3/2"
2"
5/2"
3"

Fig [illegible]

(z = -14 cm)

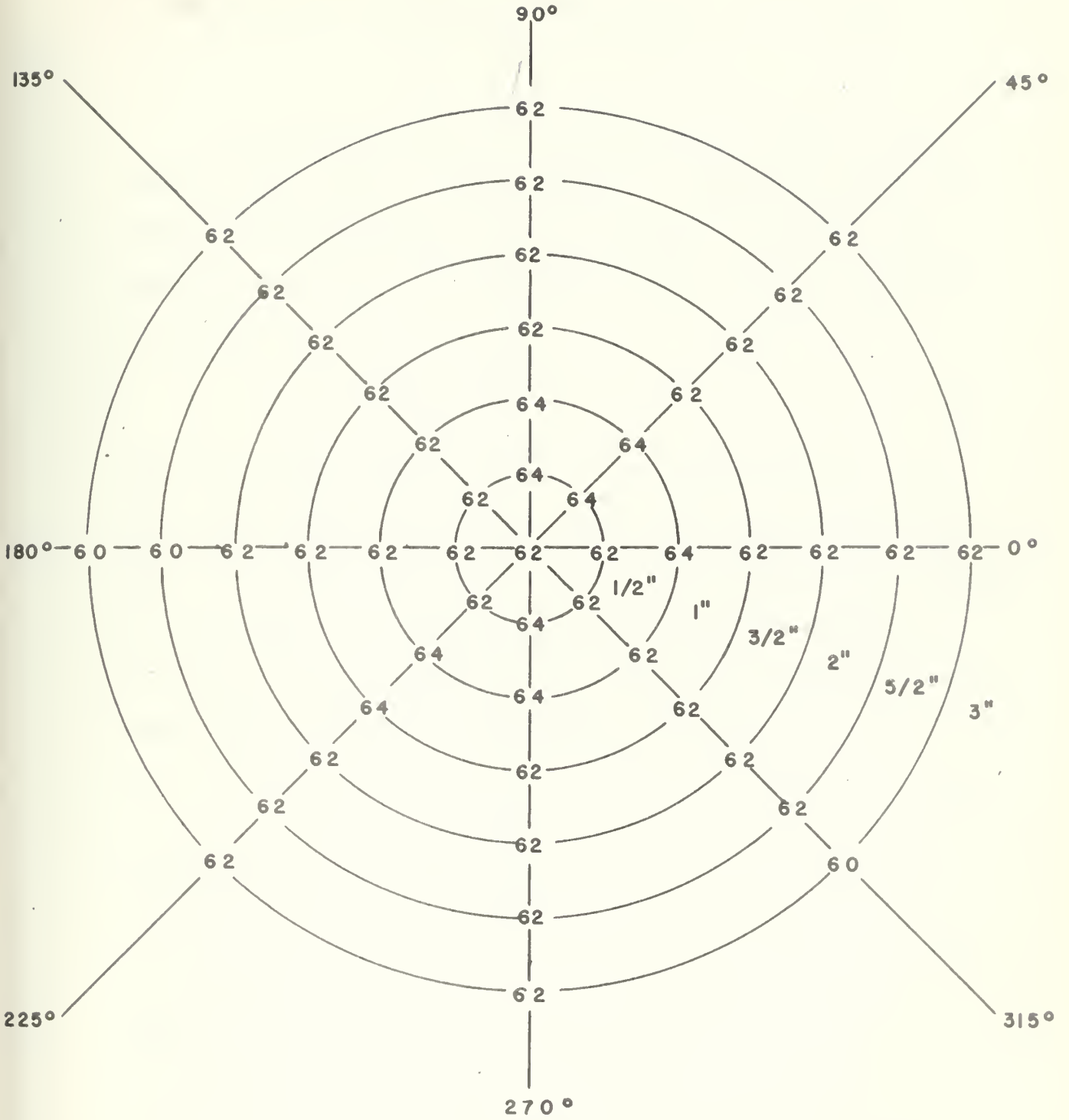

Fig. 1-5

(z = 42 cm)

Appendix 2

Derivation of Expression Relating Corrected and Measured Particle Departure Angles

The charged particle leaves the magnet axis as shown in Fig. 2-1 with an initial angle θ_c and velocity v. Assuming that near the center of the magnet where the particle leaves, the magnetic field strength is uniform, then the particle assumes a radius of curvature ρ as given by

$$\rho = \frac{m\ v\ c\ \sin\theta_c}{e\ B} \tag{2-1}$$

where all units are gaussian, and m is the particle mass, v is the initial particle velocity, θ_c is the actual particle departure angle, e is the charge of particle, B is the magnetic field strength in gauss, and c is a dimensionless factor 3×10^{10}. Because its velocity is skew to the magnetic field, the particle traverses a spiral whose radial coordinate r in plane polar coordinates is

$$r = 2\ \rho\ \sin\varphi \tag{2-2}$$

and whose axial component is given by

$$z = k\ \varphi \tag{2-3}$$

where k is the pitch of the spiral.

To find k we know that in one period T where

$$T = \frac{2\ \pi\ m\ c}{e\ B} \tag{2-4}$$

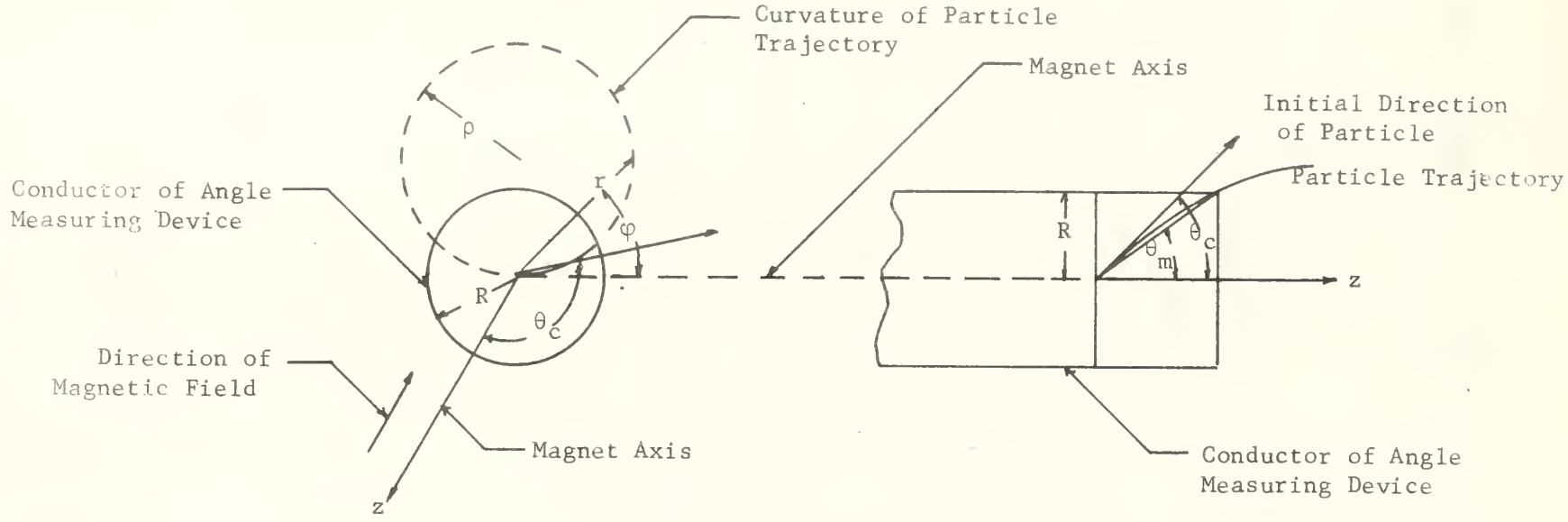

Fig. 2-1

Schematic Showing Wire Departure from Angle Measuring Device

the particle passes through $\varphi = \pi$ radians and travels an axial distance equal to

$$z = v \cos \theta_c T \quad . \tag{2-5}$$

Putting (2-4) into (2-5) and equating this to (2-3) with $\varphi = \pi$, we find that the pitch k is expressed as

$$k = \frac{2 m v c}{e B} \cos \theta_c \tag{2-6}$$

Using (2-6) we solve (2-3) for φ in terms of z with the result that

$$\varphi = \frac{z}{k} = \frac{z e B}{2 m v c \cos \theta_c} \quad . \tag{2-7}$$

Substituting (2-1) and (2-7) into (2-2) we have

$$r = \frac{2 m v c}{e B} \sin \theta_c \sin \left(\frac{e B}{2 m v c} \frac{z}{\cos \theta_c} \right) \quad . \tag{2-8}$$

Applying the boundary condition that when the wire touches the conductor of the angle measuring device

$$r = R \quad \text{and} \quad z = R \cot \theta_m \tag{2-9}$$

where θ_m is the measured particle departure angle. Letting

$$f = \frac{e B}{2 m v c} \tag{2-10}$$

we rearrange terms and derive the following transcendental equation relating the corrected and measured particle departure angles as

$$R f \csc \theta_c = \sin (f R \cot \theta_m \sec \theta_c) \quad . \tag{2-11}$$

Appendix 3

Conditions for Unique Trajectory in Uniform Field

From the differential equation describing the motion of a charged particle in a uniform magnetic field it is easy to show that

$$\frac{m v_{\perp}^2}{\rho} = e v_{\perp} B \tag{3-1}$$

where m , e , ρ , and $v_{\perp}$ is the mass, charge, radius of curvature, perpendicular component of the velocity of the charged particle respectively, and B is the magnetic field strength. Eliminating $v_{\perp}$ from the right side of (3-1) and writing

$$m v_{\perp} = m v \sin \theta_c \tag{3-2}$$

where v is the magnitude of the velocity of the charged particle and θ_c the initial angle that it makes with the field, we have

$$v \sin \theta_c = \frac{e B \rho}{m} . \tag{3-3}$$

The period T of the charged particle is given by the expression

$$T = \frac{2 \pi \rho}{v \sin \theta_c} \tag{3-4}$$

from which, upon substituting (3-3) into (3-4),we get

$$T = \frac{2 \pi m}{e B} . \tag{3-5}$$

For a given length L along the axis of the field, the charged particle will refocus back on the axis in one period providing

$$L = v \cos \theta_c T \quad . \tag{3-6}$$

Substituting (3-5) into (3-6), we have

$$L = \frac{2 \pi m v}{e} \frac{\cos \theta_c}{B} \quad . \tag{3-7}$$

Writing this expression in terms of the particle energy, we have

$$\frac{L B}{E^{\frac{1}{2}} \cos \theta_c} = \frac{2^{3/2} \pi m^{\frac{1}{2}}}{e} \quad . \tag{3-8}$$

As the right hand side is a constant, we can write (3-8) as

$$L B = K E^{\frac{1}{2}} \cos \theta_c \tag{3-9}$$

which defines any one of the four parameters L , B , E , and θ_c in terms of the remaining three. This then is the condition that determines a unique trajectory over one period in a uniform magnetic field.

Appendix 4

Particle Trajectory Measurements from Wire Orbit Method

Here θ_m is the measured departure angle, θ_c is the corrected departure angle, m is the tension, i is the wire current, E is the energy of the H_2^+ particle, I is the magnet current, z is the distance along the magnet axis, and r is the radial distance from the magnet axis.

θ_m[a] (degrees)	θ_c[a] (degrees)	m (gms)	i (amp)	E (ev)	I (amp)	z[a] (cm)	r[a] (mm)
45.48	45.78	0.86	2.0	75	6	2.5	26.0
						4.5	51.0
						6.5	69.0
						8.5	77.0
						10.0	79.0
						12.5	79.0
						14.5	78.0
						17.5	74.0
						20.5	66.0
						24.5	55.5
						27.5	45.5
						30.5	34.5
						33.5	24.5
						36.5	12.5
						40.4	0.0
47.00	47.25	0.48	2.5	84	6	2.5	27.5
						4.5	52.5
						6.5	70.5
						8.5	77.5
						10.5	80.0
						12.5	79.5
						14.5	77.5
						16.5	74.5
						19.5	67.0
						23.5	56.5
						26.5	47.0
						29.5	36.5
						32.5	26.0
						35.5	14.5
						40.4	0.0

a. See Fig. 8 for orientation of coordinate system.

θ_m	θ_c	m	i	E	I	z	r
47.85	48.10	0.57	3.0	83	6	2.5	28.0
						4.5	49.0
						6.5	70.0
						8.5	77.0
						10.5	79.0
						12.5	78.5
						14.5	76.5
						17.5	71.0
						19.5	65.5
						23.5	55.0
						26.5	43.5
						29.5	36.0
						32.0	25.5
						35.5	15.0
						40.3	0.0
49.38	49.66	0.69	3.5	89	6	2.5	30.0
						4.5	54.5
						6.5	71.0
						8.5	77.0
						10.5	79.0
						12.5	77.5
						14.5	75.0
						16.5	71.0
						18.5	66.0
						20.5	61.0
						23.5	43.0
						26.5	40.5
						29.5	37.0
						32.5	26.0
						35.5	15.0
						40.2	0.0
51.20	51.43	0.79	4.0	90	6	2.5	31.0
						4.5	56.0
						6.5	71.5
						8.5	69.5
						10.5	79.5
						12.5	79.0
						14.5	75.5
						16.5	71.5
						18.5	66.5
						20.5	61.5
						23.5	53.5
						26.5	44.5
						29.5	35.0
						32.5	25.0
						35.5	15.0
						40.0	0.0

θ_m	θ_c	m	i	E	I	z	r
51.12	51.32	0.90	4.5	92	6	2.5	31.5
						4.5	55.5
						6.5	72.0
						8.5	78.5
						10.5	79.5
						12.5	78.0
						14.5	75.5
						16.5	72.0
						18.5	67.0
						20.5	61.5
						23.5	56.0
						26.5	44.0
						29.5	34.5
						32.5	24.5
						35.5	14.0
						40.0	0.0
45.93	46.19	0.33	1.5	112	7	2.5	25.5
						4.5	47.5
						6.5	57.0
						8.5	69.5
						10.5	76.5
						12.5	77.5
						14.5	77.0
						26.5	49.5
						29.5	39.0
						32.5	28.5
						35.5	16.5
						40.4	0.0
46.18	46.48	0.41	2.0	97	7	2.5	26.0
						4.5	48.0
						6.5	64.0
						8.5	73.0
						10.5	76.0
						12.5	76.0
						14.5	74.5
						26.5	46.5
						29.5	37.0
						32.5	26.5
						35.5	16.0
						40.3	0.0

θ_m	θ_c	m	i	E	I	z	r
47.47	47.68	0.60	2.5	132	7	2.5	27.5
						4.5	50.0
						6.5	66.0
						8.5	73.5
						10.5	76.0
						12.5	75.5
						14.5	74.0
						16.5	70.5
						26.5	45.5
						29.5	36.0
						32.5	26.0
						35.5	16.0
						40.3	0.0
46.90	47.14	0.68	3.0	118	7	2.5	29.0
						4.5	52.0
						6.5	67.0
						8.5	74.0
						10.5	76.0
						12.5	75.5
						14.5	73.5
						16.5	70.0
						18.5	65.5
						20.5	61.0
						26.5	43.5
						29.5	35.0
						32.5	25.0
						35.5	14.5
						40.2	0.0
49.70	49.91	0.92	4.0	122	7	2.5	29.5
						4.5	53.5
						6.5	68.0
						8.5	75.0
						10.5	76.5
						12.5	75.5
						14.5	73.5
						16.5	69.5
						18.5	65.0
						20.5	60.0
						23.5	52.5
						26.5	43.5
						29.5	33.5
						32.5	23.5
						35.5	14.0
						40.0	0.0

θ_m	θ_c	m	i	E	I	z	r
49.48	49.68	1.08	4.5	132	7	2.5	30.0
						4.5	54.5
						6.5	69.5
						8.5	76.0
						10.5	77.5
						12.5	76.5
						14.5	74.5
						16.5	70.5
						18.5	65.5
						20.5	61.0
						23.5	53.0
						26.5	43.5
						29.5	34.5
						32.5	25.0
						35.5	15.5
						39.8	0.0
46.93	47.25	0.34	1.5	117	8	2.5	21.5
						4.5	37.0
						6.5	51.5
						8.5	60.0
						10.5	63.5
						12.5	65.0
						14.5	63.5
						16.5	60.5
						18.5	58.5
						23.5	45.5
						26.5	41.5
						29.5	33.0
						32.5	24.0
						35.5	14.5
						40.2	0.0
45.68	46.00	0.69	3.0	121	8	3.5	29.5
						5.5	44.5
						7.5	55.5
						9.5	61.0
						11.5	63.5
						12.5	64.0
						27.5	36.5
						29.5	31.0
						32.5	23.0
						35.5	14.5
						40.1	0.0

θ_m	θ_c	m	i	E	I	z	r
44.90	45.21	1.07	4.5	130	8	2.5	21.5
						4.5	39.5
						6.5	54.0
						8.5	60.5
						10.5	64.0
						12.5	64.0
						14.5	62.5
						27.5	35.0
						30.5	27.0
						33.5	19.0
						35.5	13.0
						39.8	0.0
41.42	41,71	0.44	1.5	198	9	4.5	44.5
						6.5	57.5
						8.5	65.0
						10.5	68.0
						12.5	68.5
						14.5	67.5
						16.5	65.0
						28.5	38.5
						29.5	35.0
						32.5	26.0
						35.5	16.0
						40.3	0.0
45.38	45.64	0.85	3.0	185	9	2.5	29.5
						4.5	46.0
						6.5	60.0
						8.5	67.5
						10.5	69.5
						12.5	69.0
						14.5	67.0
						16.5	64.0
						26.5	41.0
						29.5	32.5
						32.5	23.5
						35.5	14.0
						40.0	0.0

θ_m	θ_c	m	i	E	I	z	r
46.53	46.77	1.31	4.5	196	9	3.5	41.5
						5.5	57.0
						7.5	67.0
						8.5	69.5
						10.5	71.5
						12.5	70.0
						14.5	67.5
						26.5	40.0
						29.5	31.0
						32.5	22.0
						35.5	13.5
						39.8	0.0
44.18	44.47	0.47	1.5	224	10	2.5	26.5
						4.5	46.5
						6.5	61.5
						8.5	70.5
						10.5	73.5
						12.5	73.0
						14.5	71.5
						16.5	68.5
						18.5	64.5
						26.5	44.5
						29.5	46.0
						32.5	24.5
						35.5	14.0
						40.3	0.0
44.53	44.79	0.64	2.0	235	10	2.5	28.0
						4.5	37.0
						6.5	59.5
						8.5	67.0
						10.5	69.5
						12.5	69.5
						14.5	67.5
						16.5	64.5
						18.5	61.0
						25.5	45.0
						26.5	42.0
						29.5	33.5
						32.5	24.5
						35.5	15.0
						40.2	0.0

θ_m	θ_c	m	i	E	I	z	r
44.75	45.03	0.78	2.5	224	10	2.5	28.5
						4.5	46.5
						6.5	60.5
						8.5	67.0
						10.5	70.0
						12.5	69.5
						14.5	67.0
						16.5	64.0
						18.5	60.0
						23.5	49.5
						26.5	41.5
						29.5	32.5
						32.5	23.5
						35.0	15.0
						40.1	0.0
44.78	45.06	0.94	3.0	227	10	2.5	29.0
						4.5	47.5
						6.5	60.5
						8.5	58.0
						10.5	70.0
						12.5	69.5
						14.5	67.0
						16.5	63.5
						18.5	60.0
						24.5	46.0
						26.5	40.0
						29.5	31.5
						32.5	23.0
						35.0	14.0
						40.0	0.0
46.94	47.19	1.11	3.5	231	10	2.5	30.5
						4.5	51.0
						6.5	67.0
						8.5	72.0
						10.5	73.5
						12.5	72.5
						14.5	69.5
						16.5	65.5
						18.5	61.5
						24.5	46.5
						26.5	40.0
						29.5	31.5
						32.5	21.5
						35.5	12.0
						39.9	0.0

θ_m	θ_c	m	i	E	I	z	r
47.94	48.17	1.30	4.0	243	10	2.5	32.0
						4.5	52.0
						6.5	66.0
						8.5	73.0
						10.5	74.0
						12.5	72.5
						14.5	70.0
						16.5	65.0
						18.5	61.0
						26.5	40.5
						29.5	31.5
						32.5	21.5
						35.5	13.0
						39.8	0.0
49.00	49.22	1.48	4.5	250	10	2.5	33.5
						4.5	54.0
						6.5	67.5
						8.5	74.0
						10.5	74.5
						12.5	73.5
						14.5	70.5
						16.5	66.5
						18.5	62.5
						24.5	46.5
						26.5	40.5
						29.5	31.0
						32.5	21.5
						35.5	12.5
						39.7	0.0
43.17	43.44	0.54	1.5	300	11	2.5	25.5
						4.5	45.0
						6.5	58.0
						8.5	66.5
						10.5	71.0
						12.5	71.5
						14.5	68.5
						16.5	66.0
						24.5	48.0
						26.5	42.0
						29.5	35.5
						32.5	27.5
						35.5	18.5
						40.3	0.0

θ_m	θ_c	m	i	E	I	z	r
'46.38	'46.62	1.08	3.0	300	11	2.5	27.5
						4.5	47.5
						6.5	61.5
						8.5	68.5
						10.5	71.0
						12.5	70.5
						14.5	67.5
						16.5	64.5
						18.5	60.5
						26.5	40.0
						29.5	32.0
						32.5	24.5
						35.5	15.0
						39.9	0.0
47.70	47.93	1.63	4.5	301	11	2.5	31.0
						4.5	51.5
						6.5	65.0
						8.5	72.0
						10.5	74.0
						12.5	72.5
						14.5	69.5
						16.5	65.5
						27.5	36.5
						29.5	30.5
						32.5	22.0
						35.5	13.5
						39.5	0.0
44.00	44.29	0.56	1.5	320	12	3.5	35.0
						5.5	51.5
						7.5	62.5
						9.5	66.5
						11.5	69.0
						13.5	67.5
						15.5	65.5
						17.5	62.0
						27.5	36.5
						29.5	30.0
						31.5	23.0
						33.5	16.5
						35.5	10.5
						40.2	0.0

θ_m	θ_c	m	i	E	I	z	r
47.88	48.15	1.10	3.0	310	12	2.5	29.0
						4.5	48.5
						6.5	62.5
						8.5	68.0
						10.5	69.5
						12.5	69.0
						14.5	66.5
						16.5	63.0
						18.5	57.5
						25.5	41.0
						29.5	29.5
						32.5	20.0
						35.5	10.5
						39.9	0.0
49.50	49.73	1.73	4.5	340	12	4.5	52.0
						6.5	64.5
						8.5	70.0
						10.5	72.5
						12.5	71.5
						15.5	66.0
						28.5	32.0
						30.5	26.0
						33.5	16.5
						39.5	0.0
43.35	43.68	0.57	1.5	333	13	2.5	25.0
						4.5	42.5
						6.5	54.5
						8.5	62.5
						10.5	65.5
						12.5	65.5
						14.5	64.0
						16.5	61.0
						26.5	39.0
						29.5	31.0
						32.5	22.0
						35.5	13.0
						40.2	0.0

θ_m	θ_c	m	i	E	I	z	r
45.05	45.35	1.17	3.0	350	13	3.5	36.0
						4.5	44.5
						6.5	56.5
						8.5	64.0
						10.5	66.5
						12.5	66.5
						14.5	64.0
						26.5	37.5
						29.5	29.0
						32.5	20.0
						35.5	11.5
						39.8	0.0
46.50	46.75	1.85	4.5	390	13	4.5	47.5
						6.5	61.0
						8.5	67.5
						10.5	69.0
						12.5	68.0
						14.5	65.5
						27.5	35.5
						29.5	29.5
						32.5	21.0
						35.5	12.5
						39.5	0.0
43.93	44.27	0.59	1.5	357	13.75	3.5	32.5
						4.5	40.0
						6.5	51.0
						8.5	59.0
						10.5	63.5
						12.5	65.0
						14.5	64.0
						15.5	62.5
						26.5	40.0
						29.5	31.5
						32.5	23.5
						35.5	13.0
						40.2	0.0

θ_m	θ_c	m	i	E	I	z	r
46.73	46.99	1.28	3.0	420	13.75	2.5	27.0
						4.5	45.5
						6.5	58.5
						8.5	65.5
						10.5	68.0
						12.5	67.0
						14.5	64.5
						16.5	61.5
						26.5	39.0
						29.5	30.5
						32.5	22.0
						35.5	13.5
						39.9	0.0
46.47	46.73	1.94	4.5	430	13.75	2.5	29.0
						4.5	47.5
						6.5	59.5
						8.5	66.0
						10.5	68.0
						12.5	66.5
						14.5	64.0
						16.5	60.5
						24.5	42.0
						26.5	37.0
						29.5	28.5
						32.5	19.5
						35.5	10.5
						39.3	0.0